A&A 638, A82 (2020)
https://doi.org/10.1051/0004-6361/202037470

Astronomy & Astrophysics

TESS first look at evolved compact pulsators

Known ZZ Ceti stars of the southern ecliptic hemisphere as seen by TESS

Zs. Bognár[1,2,3], S. D. Kawaler[4], K. J. Bell[5,⋆], C. Schrandt[4], A. S. Baran[6], P. A. Bradley[7], J. J. Hermes[8], S. Charpinet[9], G. Handler[10], S. E. Mullally[11], S. J. Murphy[12], R. Raddi[13,14], Á. Sódor[1,2], P.-E. Tremblay[15], M. Uzundag[16], and W. Zong[17]

[1] Konkoly Observatory, Research Centre for Astronomy and Earth Sciences, Konkoly Thege Miklós út 15-17, 1121 Budapest, Hungary
e-mail: bognar@konkoly.hu
[2] MTA CSFK Lendület Near-Field Cosmology Research Group, Hungary
[3] ELTE Eötvös Loránd University, Institute of Phyiscs, Pázmány Péter sétány 1/A, 1171 Budapest, Hungary
[4] Department of Physics and Astronomy, Iowa State University, Ames, IA 50011, USA
[5] DIRAC Institute, Department of Astronomy, University of Washington, Seattle, WA 98195-1580, USA
[6] ARDASTELLA Research Group, Institute of Physics, Pedagogical University of Cracow, ul. Podchorążych 2, 30-084 Kraków, Poland
[7] XCP-6, MS F-699 Los Alamos National Laboratory, Los Alamos, NM 87545, USA
[8] Department of Astronomy, Boston University, 725 Commonwealth Ave., Boston, MA 02215, USA
[9] Institut de Recherche en Astrophysique et Planétologie, CNRS, Université de Toulouse, CNES, 14 avenue Edouard Belin, 31400 Toulouse, France
[10] Nicolaus Copernicus Astronomical Center, Bartycka 18, 00-716 Warsaw, Poland
[11] Space Telescope Science Institute, 3700 San Martin Dr., Baltimore, MD 21212, USA
[12] Sydney Institute for Astronomy (SIfA), School of Physics, The University of Sydney, Sydney, NSW 2006, Australia
[13] Dr. Remeis-Sternwarte, Friedrich-Alexander Universität Erlangen-Nürnberg, Sternwartstr. 7, 96049 Bamberg, Germany
[14] Universitat Politecnica de Catalunya, Departament de Fisica, c/ Esteve Terrades, 5, 08860 Castelldefels, Spain
[15] Department of Physics, University of Warwick, Coventry, CV4 7AL, UK
[16] Instituto de Física y Astronomía, Universidad de Valparaiso, Gran Bretaña 1111, Playa Ancha, Valparaíso 2360102, Chile
[17] Department of Astronomy, Beijing Normal University, Beijing 100875, PR China

Received 9 January 2020 / Accepted 24 March 2020

ABSTRACT

Context. We present our findings on 18 previously known ZZ Ceti stars observed by the TESS space telescope in 120 s cadence mode during the survey observation of the southern ecliptic hemisphere.
Aims. We focus on the frequency analysis of the space-based observations, comparing the results with findings of previous ground-based measurements. The frequencies detected by the TESS observations can serve as inputs for future asteroseismic analyses.
Methods. We performed standard pre-whitening of the data sets to derive the possible pulsation frequencies of the different targets. In some cases, we fit Lorentzians to the frequency groups that emerged as the result of short-term amplitude or phase variations that occurred during the TESS observations.
Results. We detected more than 40 pulsation frequencies in seven ZZ Ceti stars observed in the 120 s cadence by TESS, with precision better than 0.1 μHz. We found that HE 0532−5605 may be a new outbursting ZZ Ceti. Ten targets do not show any significant pulsation frequencies in their Fourier transforms, due to a combination of their intrinsic faintness and/or crowding on the large TESS pixels. We also detected possible amplitude or phase variations during the TESS observations in some cases. Such behaviour in these targets was not previously identified from ground-based observations.

Key words. techniques: photometric – stars: oscillations – white dwarfs

1. Introduction

A new era started in the field of variable star studies on 18 April 2018, when the Transiting Exoplanet Survey Satellite (TESS; Ricker et al. 2015) was launched successfully. As part of NASA's Explorer program, the main goal of this almost all-sky survey space mission is to detect exoplanets at nearby and bright stars with the transit method. However, with the time sampling of 30 min of the full-frame images (FFIs) provided by the satellite, and with the 120 s short-cadence mode available for selected targets, it is also possible to study the light variations of different classes of pulsating variable stars, including the pulsations of the short-period compact variables: (pre-)white dwarf and hot subdwarf stars. These later activities are coordinated by the TESS Asteroseismic Science Consortium (TASC) Compact Pulsators Working Group (WG#8).

The most populous group of pulsating white dwarf stars is also intrinsically the least luminous: the hydrogen-atmosphere

⋆ NSF Astronomy and Astrophysics Fellow and DIRAC Fellow.

Table 1. Journal of observations of the eight targets showing light variations in their TESS data sets.

Object	TIC	Start time (BJD – 2 457 000)	N	δT (d)	TESS mag	Sect.	CROWDSAP	0.1% FAP (mma)
Ross 548	029854433	1385.954	13 452	20.3	14.3	3	0.97	1.24
EC 23487−2424	033986466	1354.115	18 316	27.4	15.4	2	0.86	2.83
BPM 31594	101014997	1385.951	29 244	50.9	15.1	3–4	0.93	1.89
BPM 30551	102048288	1354.113	18 311	27.4	15.5	2	0.96	3.13
MCT 0145−2211	164772507	1385.953	13 448	20.3	15.2	3	0.98	3.00
L 19−2	262872628	1624.959	19 103	27.9	13.5	12	0.80	0.65
HE 0532−5605	382303117	1325.295	213 592	357.1	16.0	1–13	0.79	1.93
HS 0507+0434B	455094688	1437.997	17 626	26.0	15.4	5	0.40	4.23

Notes. All data were collected in 120 s cadence mode. N is the number of data points after the removal of all those with quality warning flags, δT is the length of the data sets including gaps, and Sect. is the serial number of the sector(s) in which the star was observed. The start time in BJD is the time of the first data point in the reduced data set. The CROWDSAP keyword represents the ratio of the target flux to the total flux in the TESS aperture.

pulsating white dwarfs (DAVs), named after their prototype, ZZ Ceti. These stars are short-period ($P \sim 100$–1500 s), low-amplitude ($A \sim 0.1\%$) pulsators with effective temperatures in the $T_{\rm eff} = 10\,500$–$13\,000$ K range. Pulsation modes detected in these objects are low spherical degree ($\ell = 1$ and 2), low-to-mid radial order g-modes.

A known characteristic of the ZZ Ceti pulsations is that we detect different pulsational behaviour within the temperature range that defines their instability strip. While variables closer to the blue edge (higher $T_{\rm eff}$) are more likely to show pulsational frequencies with stable amplitudes and phases, short-term (days–weeks) amplitude and phase changes are more common closer to the red edge (lower $T_{\rm eff}$). Longer periods and larger amplitudes are also detected at the cooler objects. The short-term amplitude variations can be results of the insufficient frequency resolution of the data sets, possible physical explanations include the interaction of pulsation and convection (e.g., Montgomery et al. 2010), and resonant mode coupling (e.g. Zong et al. 2016).

The *Kepler* space-telescope (Koch et al. 2010) observations revealed another unusual behaviour of these objects recently, the so-called outburst events: recurring increases in the stellar flux (up to 15%) in cool ZZ Ceti stars (see e.g. Bell et al. 2017a). This phenomenon might be in connection with the cessation of pulsations at the empirical red edge of the ZZ Ceti instability strip (Hermes et al. 2015).

For comprehensive reviews of the observational and theoretical aspects of pulsating white dwarf studies, see the papers of Winget & Kepler (2008), Fontaine & Brassard (2008), Althaus et al. (2010), and Córsico et al. (2019). For a study on the pulsational properties of ZZ Ceti stars focused mainly on space-based observations, see the paper of Hermes et al. (2017).

This paper is part of a series presenting the first results on compact pulsators based on TESS measurements. The other papers of this series focus on different types of compact variables: an sdBV (hot B subdwarf pulsator) star (Charpinet et al. 2019), another three sdBV stars (Sahoo et al., in prep.), a DBV (pulsating helium-atmosphere white dwarf) (Bell et al. 2019) and a DOV (hot hydrogen-deficient post-asymptotic giant branch) variable (Sowicka et al., in prep.).

This manuscript presents the study of 18 previously known ZZ Ceti stars bright enough to be targeted with 2 min cadence observations with TESS, observed during the survey of the southern ecliptic hemisphere. We present the 120 s cadence-mode TESS measurements collected on these stars in Sect. 2, give details on the frequency analysis of the data in Sect. 3 (both for the stars with detected light variations and those not seen to vary this time), and we discuss our findings in Sect. 4.

2. TESS observations

We downloaded the light curves from the Mikulski Archive for Space Telescopes (MAST), and extracted the PDCSAP fluxes provided by the pre-search data conditioning pipeline (Jenkins et al. 2016) from the fits files. We removed all data points with quality warning flags, and finally we corrected the light curves for long-period systematics. We normalised the light curves by fitting a fourth-order Savitzky-Golay filter with a three-day window length computed with the Python package, LIGHTKURVE (Barentsen et al. 2019). This correction does not affect the frequency domain of the short-period white dwarf pulsations. The panels of Figs. A.1 and B.1 show the resulting light curves. We note that the pre-search data conditioning pipeline corrects the flux for each target to account for crowding from other stars.

Figure A.1 shows the stars that are confirmed to vary, while Fig. B.1 shows those that do not show variability in TESS. We note that EC 23487−2424, HS 0507+0434B, Ross 548, BPM 30551, MCT 0145−2211, and L 19−2 were observed in one sector, BPM 31594 was measured in two, while HE 0532−5605, located in the TESS Continuous Viewing Zone (CVZ), was observed in 13 consecutive sectors. Tables 1 and 2 show the journal of observations of our targets seen to vary and not to vary by TESS, respectively.

3. Light-curve analysis

We performed standard Fourier analysis and pre-whitening of the data sets with the photometry modules of the Frequency Analysis and Mode Identification for Asteroseismology (FAMIAS) software package (Zima 2008)[1]. We also used in-house developed software for the least-squares fitting, used for the analysis of Whole Earth Telescope (Nather et al. 1990),

[1] FAMIAS is a package of software tools for the analysis of photometric and spectroscopic time-series data. It enables us to search for periodicities in these data sets using the method of Fourier analysis and non-linear least-squares fitting techniques. FAMIAS is also capable of performing mode identification of the detected periodicities utilising different photometric and spectroscopic methods.

Table 2. Journal of observations of the targets not seen to vary by the TESS data sets.

Object	TIC	Start time (BJD – 2 457 000)	N	δT (d)	TESS mag	Sect.	CROWDSAP	0.1% FAP (mma)
MCT 2148−2911	053851007	1325.301	18 094	27.9	16.1	1	0.17	6.19
HE 0031−5525	281594636	1354.113	18 313	27.4	15.8	2	0.28	5.47
EC 00497−4723	101916028	1354.113	18 315	27.4	16.5	2	0.85	8.35
MCT 0016−2553	246821917	1354.114	18 317	27.4	15.9	2	0.13	4.92
WD 0108−001	336891566	1385.954	13 451	20.3	17.0	3	0.92	10.93
HS 0235+0655	365247111	1410.908	15 751	25.9	16.5	4	0.89	12.42
KUV 03442+0719	468887063	1437.997	17 631	26.0	16.6	5	0.57	16.62
WD J0925+0509	290653324	1517.403	13 384	24.6	15.3	8	0.56	3.81
HS 1013+0321	277747736	1517.402	13 390	24.6	15.7	8	0.97	4.59
EC 11266−2217	219442838	1544.278	15 569	24.2	16.4	9	0.35	5.20

Table 3. Periods and frequencies derived by ground-based observations on Ross 548.

	Period [s]	Frequency [μHz]	Amplitude [mma]	Amplitude at 825 nm
f_1	212.8	4699.2	4.28(4)	2.71
f_2	213.1	4692.6	6.86(4)	4.34
f_3	274.3	3646.3	4.41(4)	2.79
f_4	274.8	3639.4	3.17(4)	2.01

Notes. The next-to-last column lists the corresponding weighted mean amplitudes (near V magnitude), while the last column is the expected amplitude in the TESS band pass assuming a black-body-spectral-energy distribution as per Eq. (1).

Kepler, and K2 data. We chose the detection limit to be at 0.1% false alarm probability (FAP), and, in this case, there is a 99.9% chance that a peak reaching this limit is not just a result of noise fluctuations.

We calculated the 0.1% FAP threshold following the method described in Zong et al. (2016): we generated 10 000 synthetic light curves of Gaussian random noise for the times of the real observations, calculated their Fourier transforms up to the Nyquist limit (≈4167 μHz), and then determined the probability for the different signal-to-noise (S/N) ratios that a single peak emerges at that S/N value only due to noise fluctuations. The noise level was chosen to be the mean amplitude level of the given synthetic light curve. This way, we were able to calculate the S/N values corresponding to the 0.1% FAP thresholds, and we accepted a frequency peak only above this S/N limit as significant.

In some cases, we were unable to remove all of the observed power by simple pre-whitening, suggesting the presence of amplitude or phase variations in the signal. We fit Lorentzian envelopes to these peaks as described in Bell et al. (2015) and Hermes et al. (2017). We fit the peaks in the power spectrum with the function presented in Eq. (1) of Bell et al. (2015) and Eq. (1) of Hermes et al. (2017). The Fourier transforms were oversampled by a factor of six.

3.1. Ross 548

Ross 548 (TIC 29854433, $G = 14.23$ mag[2], $\alpha_{2000} = 01^{\rm h}36^{\rm m}14^{\rm s}$, $\delta_{2000} = -11^{\rm d}20^{\rm m}33^{\rm s}$) is also known as ZZ Ceti, and it is the namesake of the class of hydrogen-atmosphere pulsating white dwarfs.

[2] *Gaia* Data Release 2 G magnitude, Gaia Collaboration (2018).

3.1.1. Ground-based observations

Ross 548 was one of the first pulsating white dwarfs discovered by Lasker & Hesser (1971). The star has shown a remarkably stable pulsation spectrum for over 48 years, with two dominant periodicities (each now known to be triplet ($\ell = 1$) modes). Lasker & Hesser (1971) isolated two modes with periods of 212.864 s (4697.8 μHz) and 273.0 s (3663 μHz). These relatively short periods are consistent with its position near the blue edge of the ZZ Ceti instability strip, with an effective temperature of 12 200 K (Giammichele et al. 2015, and references therein).

The stability of the pulsation amplitudes and frequencies has been studied in depth, in part to determine the secular period change rates driven by the cooling of the star. This decades–long effort is summarized in, for example, Mukadam et al. (2013). The two main modes identified by Lasker & Hesser (1971) have been resolved as triplets, with the amplitude of the central $m = 0$ peak about 3−5 times smaller than the flanking $m = \pm 1$ peaks. The splitting is 4.0 μHz for the 213 s mode, and 3.5 μHz for the 275 s mode.

Mukadam et al. (2013) reported that the amplitudes of the $m = \pm 1$ modes in Ross 548, have been very stable: a fact that has enabled the measurement of the long–term secular change in the pulsation phase, and therefore the rate of period change. This decades-long stability in principle allows us to use Ross 548, to help calibrate the pulsation amplitudes of white dwarfs observed by TESS without having simultaneous ground-based observations.

In Table 3, we present the weighted average amplitudes of the largest-amplitude modes in Ross 548. Amplitudes we used are those reported by Giammichele et al. (2015), Mukadam et al. (2013), and references therein.

The band pass of TESS is much redder than that of ground-based photomultiplier and CCD observations, but we can compute the expected amplitude in the TESS band pass quite readily.

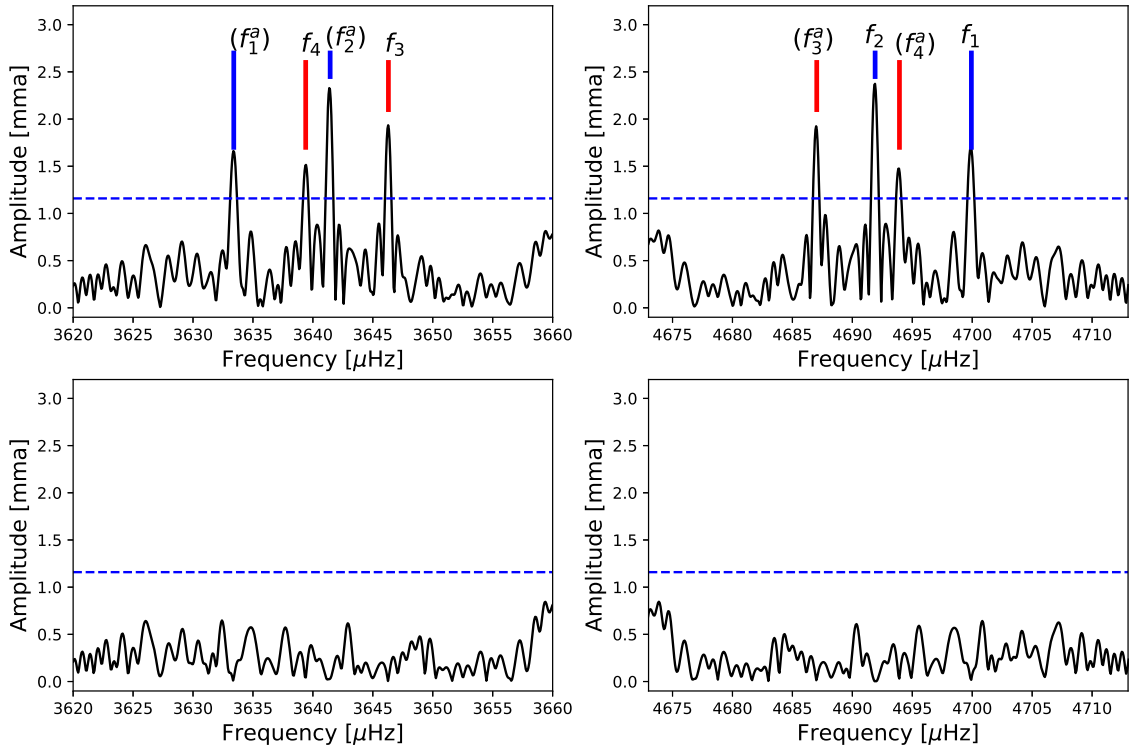

Fig. 1. Fourier transform of TESS light curve of Ross 548. *Left panels*: sub-Nyquist frequency range where the signal exceeds the 0.1% FAP (S/N = 4.54, horizontal dashed line). The peaks correspond to f_3 and f_4 from Table 3 (red lines), and the aliases (reflected across the Nyquist frequency) of f_1 and f_2 (blue vertical lines). *Right-hand panels*: transform above the Nyquist frequency, where the real periodicity – alias situation is reversed. *Two bottom panels*: residuals in the spectrum after pre-whitening by the least-squares fit sinusoids f_1, f_2, f_3, f_4 listed in Table 4.

Table 4. Weighted mean amplitudes (from ground-based photometry) for the dominant pulsation modes in Ross 548.

	Period [s]	Frequency [μHz]	Amp [mma]	TESS pred [mma]	TESS obs [mma]
f_1	212.7704(17)	4699.900(37)	4.28(4)	1.82(2)	1.3(2)
f_2	213.1348(12)	4692.868(26)	6.86(4)	2.93(2)	2.4(2)
f_3	274.2521(24)	3646.280(32)	4.41(4)	2.42(2)	1.9(2)
f_4	274.7719(28)	3639.383(37)	3.17(4)	1.74(2)	1.8(2)

Notes. The fifth column shows the amplitude expected in the TESS band pass, corrected for amplitude dilution near the Nyquist frequency.

Since the g-mode pulsations reflect temperature changes across the white dwarf surface, we can (assuming a black body with $T \approx 12\,200$ K) compute the amplitude ratio in the TESS band pass (centered at approximately 825 nm) to that in the optical (assumed to be 425 nm), following Kawaler et al. (1994):

$$\frac{A_{825}}{A_{425}} = \frac{425}{825}\, e^{-16450/T}\, \frac{e^{33890/T} - 1}{e^{17458/T} - 1}. \quad (1)$$

For $T_{\rm eff} = 12\,200$ K, this implies that the amplitudes observed by TESS should be about 63% of those observed in the optical. The last column in Table 3 therefore shows the expected amplitudes for TESS observations. We compiled the published observed amplitudes of Ross 548, to obtain an estimate of the expected amplitude for our observations with TESS.

3.1.2. TESS observations

TESS observed Ross 548, during Sector 3. The light curve is shown in Fig. A.1. We note that toward the end of the first segment, the noise level in the light curve increased (a common issue for Sector 3 data). We chose to retain those data to improve the duty cycle after examining the periodogram with and without the problematic segment to ensure that the noise did not adversely impact the frequency analysis.

Our 0.1% FAP level is at an S/N of 4.59 (corresponding to an amplitude of 1.24 mma). In the periodogram, the only peaks that rose above that threshold were precisely at the frequencies corresponding to the known pulsation modes (or their Nyquist aliases) listed in Table 3. While the 275 s modes (at 3646.3 and 3639.4 μHz) were below the Nyquist frequency of 4167 μHz, the 213 s modes (at 4692.6 and 4699.2 μHz) are above the Nyquist frequency. They are "reflected" back across the Nyquist frequency to 3640.7 and 3634.1 μHz. As we show in Fig. 1, the two aliases of the 213 s modes intermingle with the two 275 s peaks. Beyond the Nyquist frequency, the same pattern repeats, with the alias of the 275 s modes intermingling with the "true" 213 s peaks. We performed a least-squares fit to the time series of Ross 548 using the prior values of the four frequencies as a starting point. The formal fit to the light curve is given in

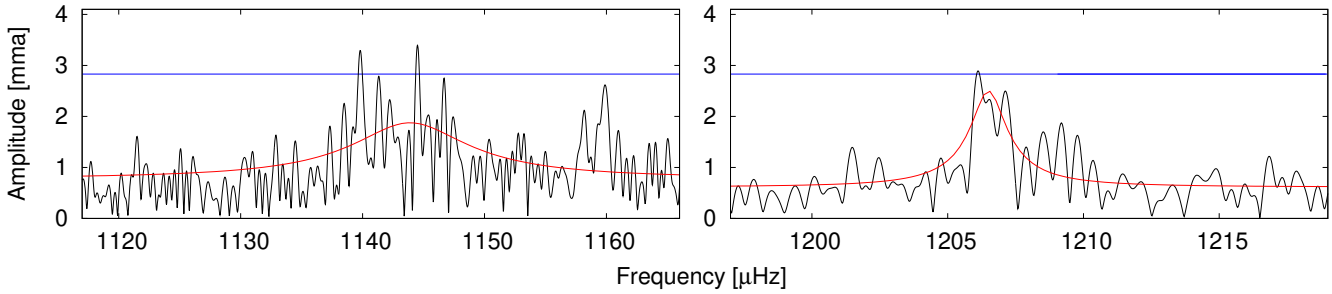

Fig. 2. Lorentzian fits (red lines) to frequency regions at 1143 and 1206 μHz. Blue lines denote the 0.1% FAP level.

Table 4. Pre-whitening the data using these four frequencies completely removes all peaks in this region, and their mirror aliases, at or near the 0.1% FAP. For more details considering the super-Nyquist analyses of compact pulsators, see the papers of Baran et al. (2012) and Bell et al. (2017b).

Finally, for comparison with the ground-based measurements of the amplitudes of the modes of Ross 548, we need to correct the fit values of the amplitudes for the fact that the frequencies lie close to (and beyond) the Nyquist frequency. Thus the signals are attenuated by the smoothing/averaging over the 120 s TESS integrations. Assuming a sinusoidal waveform, the functional form of the attenuation is a sinc function in frequency, with the first zero at twice the Nyquist frequency. The corrected amplitudes are in the fifth column of Table 4. The corrections were applied to the uncertainties, and the ground-based optical amplitudes were reduced by the band pass and integration near the Nyquist limit to compare with the TESS observed values.

Considering the 11-frequency solution presented by Giammichele et al. (2015), we found that only the four highest amplitude modes can be seen in the TESS data set. The rest, with ground-based amplitudes of 0.3–1.4 mma, all fall below the detection limit.

Comparing the (corrected) observed amplitudes from TESS to the expected values from ground-based data over the past 48 years, we see that there is close agreement for all four modes resolved by TESS. Therefore, we expect that amplitudes from TESS can be directly compared with archival and future ground-based measurement of the amplitude of white dwarf pulsations (after correcting for different band passes and exposure times).

3.2. EC 23487−2424

The light variations of EC 23487−2424 (TIC 033986466, G = 15.38 mag, α_{2000} = $23^{\rm h}51^{\rm m}22^{\rm s}$, δ_{2000} = $-24^{\rm d}08^{\rm m}17^{\rm s}$) were discovered by Stobie et al. (1993).

3.2.1. Ground-based observations

Stobie et al. (1993) revealed a complex frequency structure by their six-night measurements. They determined four pulsation frequencies at 1007.07, 1243.07, 1151.79, and 1010.86 μHz (992.98, 804.46, 868.21, and 989.26 s, respectively). They also detected the second harmonics of several frequencies, and additional closely spaced frequency components at the 1010.86 μHz peak. Apart from the discovery paper, the results of only one observation have been published up to now: Thompson et al. (2005) presented a two-frequency solution with periods at 878.8 and 508.1 s, based on time-series spectroscopy.

3.2.2. Results of the TESS observations

If we pre-whiten the data set with the standard procedure down to the significance threshold, we can identify 17 frequencies above the 0.1% FAP limit (S/N = 4.74). However, these are not all independent pulsation modes, but they form groups of peaks in some cases, suggesting amplitude or phase variations occurring during the TESS observations. In actual fact, we found that the high-frequency peaks (those with periods shorter than 800 s) are stable enough in amplitude and phase that pre-whitening leaves no residuals above the detection threshold. However, significant residuals remain after removing the lower frequency peaks.

This feature is consistent with Fig. 5 of Hermes et al. (2017), which shows the stochastic nature appearing at periods longer than about 800 s. Therefore, we fit a Lorentzian envelope to the regions at 1144 and 1206 μHz (see Fig. 2). The dominant frequency at 1367 μHz (~730 s) shows intermediate behavior – removing the main peak leaves behind some additional peaks, but that one peak's dominance makes fitting a Lorentzian challenging. The damping times calculated for the 1144 and 1206 μHz regions are 0.183 and 2.252 days with Lorentzian widths of 25.5 ± 1.0 μHz and 1.59 ± 0.11 μHz, respectively.

Table 5 lists the results of the ten-frequency fit, including the parameters of the Lorentzian fits, while Fig. 3 shows the Fourier transform of the whole light curve. Red dashed lines mark the frequencies listed in Table 5.

We note that the dominant peak and the peaks at 1372.116 and 1376.720 μHz form a triplet with 5.034 and 4.604 μHz frequency separations, respectively, while we see similar frequency difference of 4.085 μHz between the peaks at 1143.895 and 1139.810 μHz. This suggests that we see the results of rotational frequency splitting at least in the first case. Considering the 4.085 μHz separation, the approximate rotation period of the star could be 1.42 or 2.36 d, assuming the rotational splitting of ℓ = 1 or ℓ = 2 modes, respectively.

In Table 5, we also mark the frequencies obtained by ground-based observations. Apparently, Stobie et al. (1993) detected a set of modes completely different from those we determined by the TESS observations, as if we observed two different stars. Besides the detected complex frequency structure with closely spaced peaks in the Fourier transforms, this also suggests that some of the mode amplitudes are not stable.

3.3. BPM 31594

The star BPM 31594 (TIC 101014997, G = 15.06 mag, α_{2000} = $03^{\rm h}43^{\rm m}29^{\rm s}$, δ_{2000} = $-45^{\rm d}49^{\rm m}04^{\rm s}$) was discovered as the tenth member of the ZZ Ceti class by McGraw (1976).

Table 5. This work: results of the fit of the EC 23487−2424 data set with ten frequencies.

	This work			Stobie et al. (1993)	Thompson et al. (2005)
	Frequency [μHz]	Period [s]	Ampl. [mma]	Period [s]	Period [s]
				993.0	
				989.3	
$f_1^{-1/0}$	1139.799(34)	877.348	3.30(49)		878.8
$f_1^{0/+1}$	1144.67(35)*	873.614	1.61(30)		
				868.2	
f_2	1206.495(39)*	828.847	2.41(05)		
				804.5	
f_3^{-1}	1367.082(17)	731.485	6.65(49)		
f_3^{0}	1372.116(35)	728.802	3.15(49)		
f_3^{+1}	1376.720(39)	726.364	2.81(49)		
f_4	1430.780(17)	698.920	6.41(49)		
f_5	1589.850(37)	628.990	2.96(49)		
f_6	1708.434(27)	585.331	4.05(49)		
f_7	1963.783(23)	509.221	4.88(49)		508.1

Notes. The errors are formal uncertainties. The results of Lorentzian fits are marked with star symbols (*). In the case of the supposed rotationally split frequencies, we mark the possible azimuthal order values. For completeness, we also list the periods detected by Stobie et al. (1993) and Thompson et al. (2005).

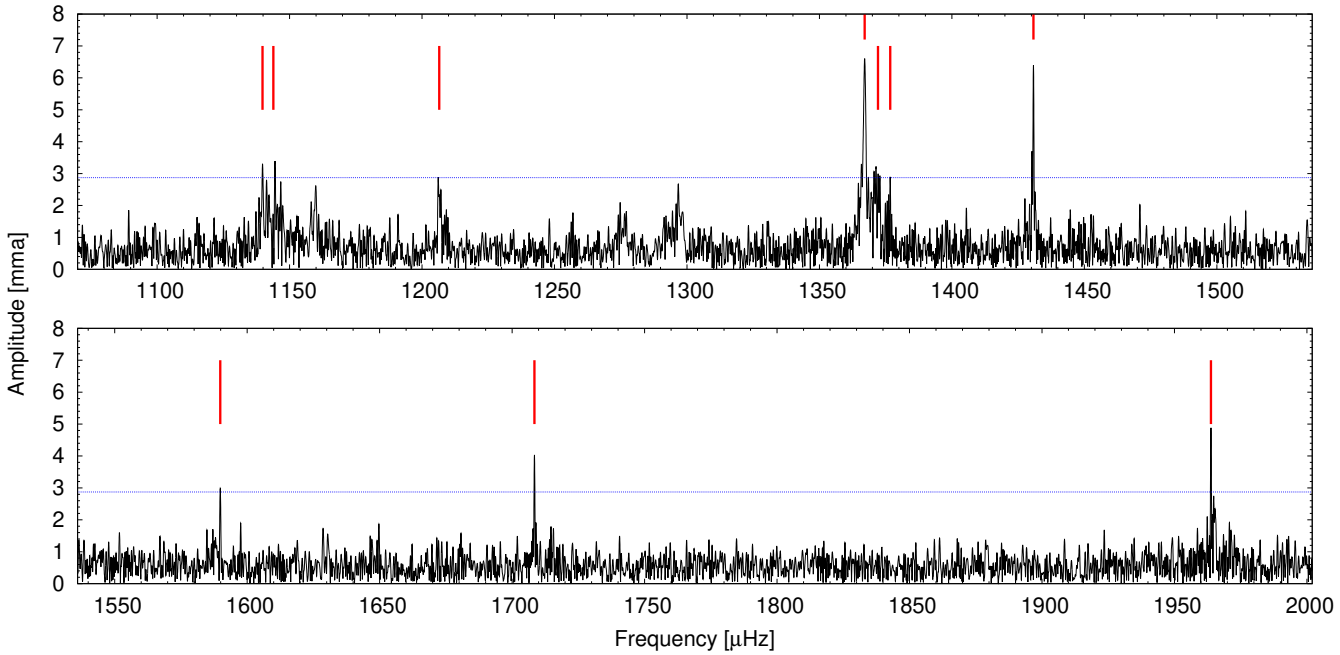

Fig. 3. Fourier transform of light curve of EC 23487−2424. Red lines mark the frequencies listed in Table 5, while the blue dashed line represents the 0.1% FAP level ($S/N = 4.74$) calculated by this Fourier transform.

3.3.1. Ground-based observations

McGraw (1976) presented the results of four nights of observations. They reported an interesting change in the pulsational behaviour of BPM 31594. On the discovery night, it showed light variations with 314 s, but on the subsequent nights, its periodicity changed to 617 s. However, it later turned out that this change was not real, but only a result of erroneous data reduction of the first night's measurements (Odonoghue 1986). McGraw (1976) also detected the two harmonics of the 617 s mode (f_0), significant power in the spectra near $(3/2)f_0$, and combinations of frequencies.

O'Donoghue et al. (1992) presented the results of the long-term investigations of BPM 31594 carried out between 1975 and 1989. They found the dominant frequency to be at $f_0 = 1.62$ mHz (617 s) again, and detected significant peaks at multiples of $1.54 f_0$. In some cases, further frequencies appeared at multiples of $1.48 f_0$. They also identified, that at f_0 there is actually a rotationally split triplet with 12.7 μHz frequency separations. Besides these, they detected the harmonics of f_0, an additional frequency at 1.8778 mHz (533 s), and several combination terms. Considering the stability of frequencies, they found variability in the period of f_0, and also variable amplitudes at the other frequencies from season to season. The authors

Table 6. 14-frequency solution of the BPM 31594 data set.

	Frequency [μHz]	Period [s]	Amplitude [mma]
$f_3 - f_3^{\pm1}$	13.409(12)	74577	3.08(32)
f_1	1461.117(13)	684.408	2.87(32)
f_2	1548.455(4)	645.805	8.47(32)
f_3^{-1}	1604.982(4)	623.060	8.94(32)
f_3	1618.401(1)	617.894	39.37(32)
f_3^{+1}	1631.844(4)	612.804	10.80(32)
f_w	2483.203(7)	402.706	5.06(32)
$1.54 f_3$	2490.147(7)	401.582	5.35(32)
$f_2 + f_3$	3166.877(9)	315.769	4.05(32)
$2f_3$	3236.794(6)	308.948	6.26(32)
f_x	3245.648(11)	308.105	3.41(32)
f_y	3252.590(12)	307.447	3.16(32)
$2.54 f_3$	4108.584(15)	243.393	2.49(32)
f_z	4115.083(16)	243.009	2.41(32)

Notes. The errors are formal uncertainties calculated by FAMIAS. In the case of the rotationally split frequency, we mark the azimuthal order values.

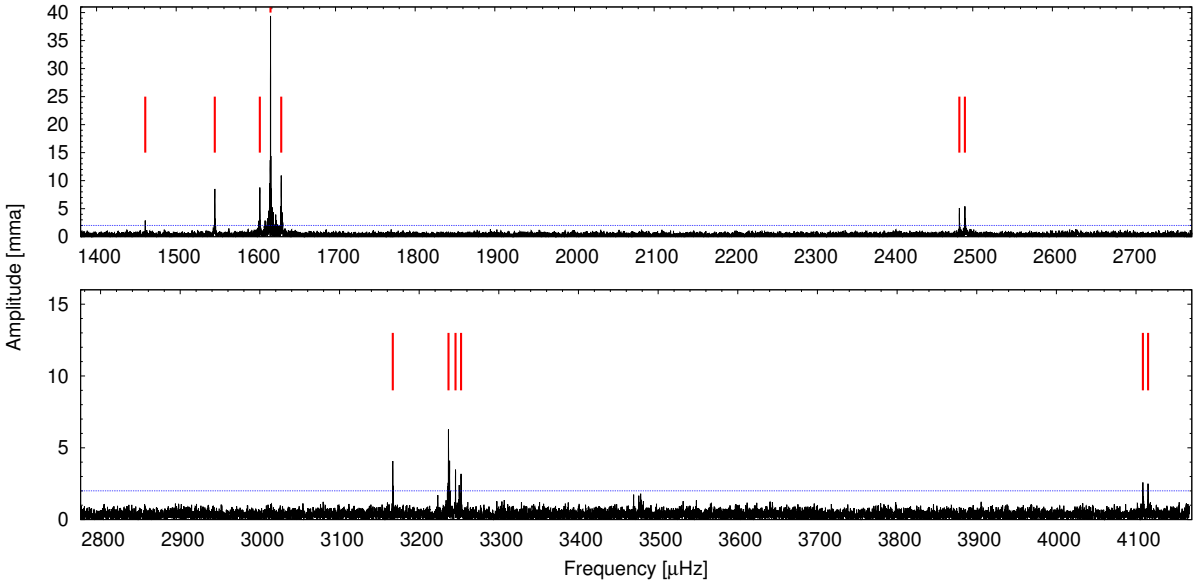

Fig. 4. Fourier transform of light curve of BPM 31594. Red lines mark the frequencies listed in Table 6, while the blue dashed line represents the 0.1% FAP level (S/N = 4.85) calculated by this Fourier transform.

summarised their findings as the observed structure of the frequencies of BPM 31594 can be described by only a few independently excited modes, which drive others through nonlinear coupling by direct resonance.

3.3.2. TESS observations

The dominant peak is at 1618.405 μHz, in agreement with the results of the previous observations. This peak is also the central component of a triplet with 13.42 μHz frequency separations. This is also in good agreement with the 12.7 μHz finding of O'Donoghue et al. (1992) by ground-based observations. We note that there are also residual closely spaced peaks at the triplet components. These are partly caused by the (apparent) changing noise level between the two sectors and sub-sector parts.

We also detected the second harmonic of the dominant frequency, significant peaks at 1.54 and 2.54 times the dominant frequency, two independent frequencies at 1461.119 and 1548.455 μHz, a combination term at 3166.876 μHz, and a low-frequency peak corresponding to the frequency separation of the triplet components at 13.409 μHz.

Table 7. Consistent periodicities in the ground-based observations of BPM 30551 determined by Hesser et al. (1976).

	Frequency [μHz]	Period [s]	Amplitude range [mma]
f_1	1643.1	608.6	12–15
f_2	1464.8	682.7	10–12
f_3	1342.8	744.7	7
f_4	1190.2	840.2	15
f_5	1159.7	862.3	6–15

Besides these, four additional peaks can be determined by the data set, close to, but well-separated from the peaks at 1.54, 2, and 2.54 times the dominant peak, respectively. These are at f_w = 2483.202, f_x = 3245.652, f_y = 3252.593, and f_z = 4115.083 μHz. It is remarkable that the spacing between

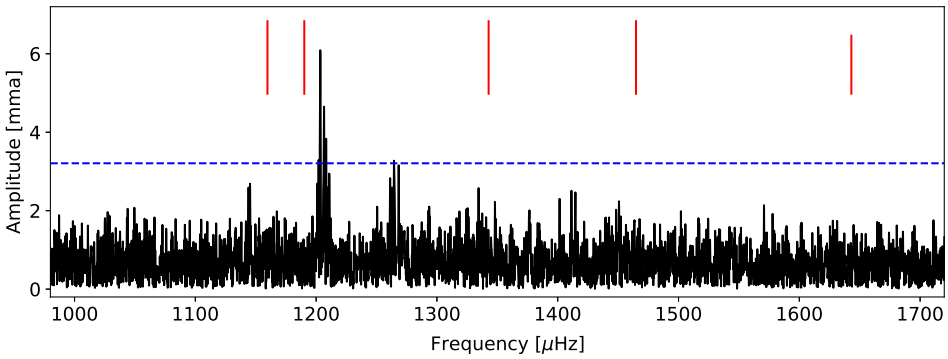

Fig. 5. Fourier transform of light curve of BPM 30551 in the only spectral region where signals reached above the 0.1% FAP level (S/N = 4.69, blue dashed line). Red lines mark the approximate frequencies seen in the 1975 data reported in Hesser et al. (1976) and listed in Table 7.

f_w and $1.54 f_1$ is 6.952 μHz, which is nearly half the spacing within the triplet around the dominant peak. This is also true for the spacings between f_x and f_y (δf = 6.941 μHz), and f_z and $2.54 f_1$ (δf = 6.50 μHz). The origin of these additional peaks is in question.

Table 6 lists the 14-frequency solution without the closely spaced residual peaks (the 0.1% FAP limit is S/N = 4.85). These frequencies are also marked in Fig. 4, showing the Fourier transform of the whole light curve.

3.4. BPM 30551

The star BPM 30551 (TIC 102048288, G = 15.48 mag, α_{2000} = $01^h06^m54^s$, δ_{2000} = $-46^d08^m54^s$) was one of the first ZZ Ceti pulsators discovered; the first observations are described by Hesser et al. (1976).

3.4.1. Ground-based observations

Hesser et al. (1976) identified several periodicities between 1190 and 1640 μHz in 24 observing runs spanning several months. The power spectrum was variable, but most of the peaks in the Fourier transforms of individual runs were situated in the 1000–1900 μHz domain (see Table 7). In retrospect, we recognise this as typical behaviour of cool DAV stars, with complex pulsation spectra of modes with periods longer than 800 s (Hermes et al. 2017). To our knowledge, no time-series photometric observations of BPM 30551 have been performed since the discovery observations in 1974. Given this, the low-resolution Fourier transforms available in Hesser et al. (1976) make it difficult to compare with the TESS results.

3.4.2. TESS observations

The star BPM 30551 was observed for 25.4 days during the 27.5 day observation of Sector 2, so therefore with a duty cycle of 92.5%. The light curve of BPM 30551 (see Fig. A.1) shows no evidence for bursts, which occur in some DA white dwarfs that pulsate in similar periods (Bell et al. 2016). There were no apparent low-frequency variations (1 day or longer) following examination of the unflattened light curve.

The Fourier transform of the light curve of BPM 30551 – the first observations since the mid 1970s – confirms that it is indeed a DAV pulsator, with the largest-amplitude variations at frequencies between 1100 and 1300 μHz. Figure 5 shows the FT over the range of frequencies reported by Hesser et al. (1976), with red lines showing the approximate positions of their identifications. In the TESS data, the only significant signals (i.e., S/N above 4.69) are in a narrow frequency range between 1195 and 1215 μHz, with a second region around 1260 μHz that lies just above the significance threshold.

An expanded view of the FT of the BPM 30551 data is shown in Fig. 6. The signal in the range from 1200–1215 μHz is extremely complex, indicating that the mode or modes of pulsation are not coherent over the 27 day duration of the run. In fact, this is very similar to what is seen in the longer period pulsations of DAV stars near the cool end of the instability strip, which is reminiscent of stochastically driven oscillations seen in solar-type asterosesimic data. Attempts to identify and remove coherent periodicities in this region were unsuccessful. Pre-whitening was not sufficient to remove all of the observed power, and as individual coherent periodicities were removed, new nearby peaks appeared. Therefore, we fit a Lorentzian envelope to this region and the region around 1260 μHz. The central frequencies of the Lorentzian fits to the frequency groups are as follows: 1204.17 ± 0.02 μHz, and 1264.49 ± 0.16 μHz. We note that, as Fig. 6 shows, we can fit a third frequency group at ~1140 μHz with the central frequency at 1144.75 ± 0.15 μHz, even though the corresponding peaks are below our detection threshold (Table 8).

We find a damping time for the strongest modes of about 0.77 days; thus the 27 day observing span dilutes the true power of the oscillations over a broad range of frequencies. Shorter observations, such as a typical one-night terrestrial observation, which is shorter than the typical damping time for these modes, would be expected to see much larger amplitude pulsations. Indeed, simulations show that modes that conform to the fitted Lorentzian power envelope widths and heights can produce peaks in excess of 20 mma within that frequency range. Thus the results from Hesser et al. (1976) are consistent with what TESS observed. However, the modes seen by Hesser et al. (1976) at other frequencies are (apparently) either too low in amplitude to be detected, or are no longer present.

3.5. MCT 0145−2211

The pulsating behaviour of the DAV MCT 0145−2211 (TIC 164772507, G = 15.23 mag, α_{2000} = $01^h47^m22^s$, δ_{2000} = $-21^d56^m51^s$) was announced concurrently with HE 0532−5605 in Fontaine et al. (2003).

3.5.1. Ground-based observations

It was observed over two consecutive nights for 3740 s on the first and 5780 s on the second, each with sampling times of 10 s (Fontaine et al. 2003). They identified three periodicities at 1215, 1374, and 2164 μHz with amplitudes ranging from 17 to 25 mma; they noted that they expected that more periods could likely be resolved with longer observations. They determined

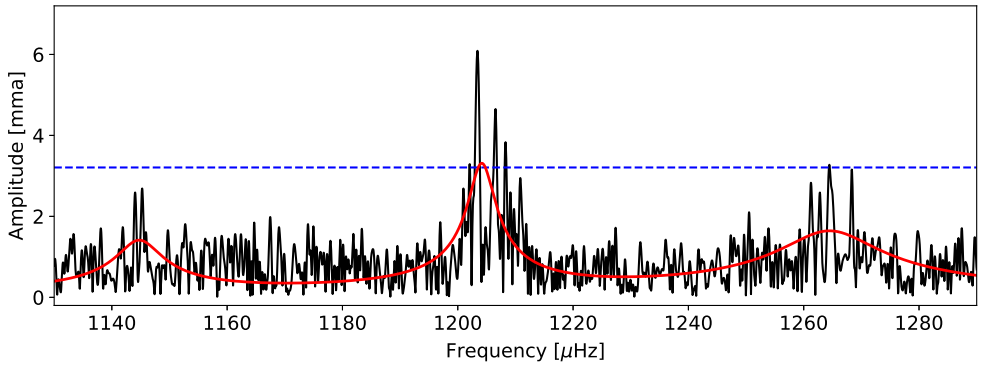

Fig. 6. Area of maximum signal in Fourier transform of BPM 30551. The region of largest signal is complex. The red curve is a fit of Lorentzian envelopes to the main signal, and the two flanking regions that do not reach the significance threshold.

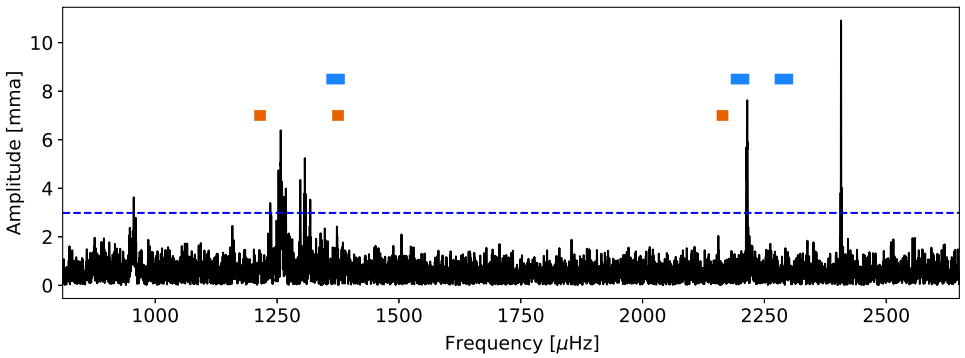

Fig. 7. Fourier transform of TESS light curve of MCT 0145−2211; the blue dashed line indicates the 0.1% FAP level (S/N = 4.57). Red bars mark the frequencies reported by Fontaine et al. (2003), and blue bars above mark those noted by Kilkenny et al. (2014).

the temperature of the star to be around 11 550 K, making this another example of a DAV being in the middle of the instability strip.

These observations were followed up by Kilkenny et al. (2014). They observed for 50 min with a sampling time of 0.1 s. The frequency resolution of their data was approximately 8 μHz, estimated using their data and Eq. (5.52) of Aerts et al. (2010). They identified three periodicities in this short data set at 1370, 2200, and 2290 μHz with amplitudes between 6 and 10 mma which, given the brevity of their observations, are consistent (in frequency) with two of the three identified by Fontaine et al. (2003).

3.5.2. TESS observations

From the TESS light curve, we see that MCT 0145−2211 is still pulsating, with periodicities that are in the same range as reported earlier. However, some differences with the earlier data are evident. The highest peak in the FT in Fig. 7 is a single, fully resolved peak at 2407.20 μHz, with an amplitude of 11 mma, which was not seen in the earlier work. In this context, a frequency is considered resolved when it is a single peak that can be pre-whitened with a sinusoid. The second-highest peak(s) lie between 2212 and 2216 μHz, consistent with what was reported earlier. There are at least three peaks within this frequency range, but the 20.3 day span of Sector 3 data on this star was not long enough to fully resolve them. Least-squares fits and pre-whitening in this frequency range revealed at least three closely spaced but unresolved modes.

At lower frequencies, the TESS data show several groups of significant peaks that fall within roughly Lorentzian envelopes, at 956 μHz, 1257 μHz and 1306 μHz (periods of 1046 s, 796 s, and 766 s). As with the other cool DAVs in this study, we were unable to completely pre-whiten peaks within these three regions, indicating that the modes may be amplitude or phase unstable over the span of the observations. In Fig. 8, we expand the view around several peaks, and show the residuals after removing the largest peaks in each range. This illustrates that the 2407.20 μHz mode is a single coherent periodicity, while the modes with frequencies below 1400 μHz are complex. The 2215 μHz mode seems under-resolved: we can find four frequencies using a least-squares sinusoidal fitting that removes most of the peak, but the frequencies are separated by small amounts that are nearly at the expected resolution for a run of this length.

In summary, the only resolved, coherent oscillation can be fit with a sinusoid with a frequency of 2407.200 ± 0.014 μHz, with an amplitude of 10.9 ± 0.6 mma. Considering the mode near 2215 μHz, there is insufficient time to resolve this into individual peaks, and therefore we can not yet say if this is a stochastically excited mode or if it is a closely spaced multiplet. If it is a closely spaced multiplet, and rotation is what causes the splitting, then it would be one of the most slowly rotating white dwarfs with asteroseismic results as per Hermes et al. (2017).

There seems to be a "triplet" at 1305.215, 1306.980, and 1308.724 μHz (all about ±0.04 μHz) though all three are close to the false-alarm limit. A 1.7 μHz splitting corresponds to a rotation period of 3.3 days if that triplet is indeed associated with an ℓ = 1 mode. The peaks on either side of that triplet at 1297.55 and 1317.98 are nearly equally spaced around that 1307 μHz clump. However, the three peaks close to 1307 μHz are not a triplet, but a single stochastically excited mode, and the 1298 and 1318 μHz to either side make up the rest of the (more widely spaced) triplet that would be present if the rotation period were 0.57 days. We were unable to get a satisfactory fit using Lorentzians for that wider triplet case.

As we mentioned above, there are two additional frequency regions with peaks at 956 and 1257 μHz, respectively. We note that they are also not resolved, and they are all close enough to the significance threshold (Table 9).

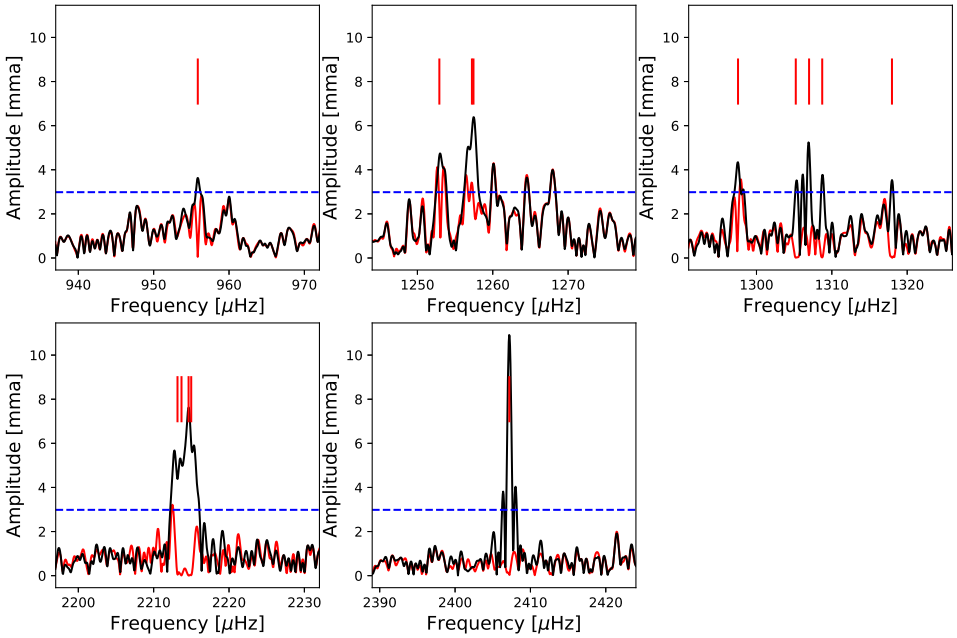

Fig. 8. Fourier transform of TESS light curve of MCT 0145−2211; the blue dashed line indicates the 0.1% FAP level (S/N = 4.57). Red bars mark the frequencies obtained by a successive least-squares fitting and pre-whitening process. Residuals after pre-whitening are shown as the red curve.

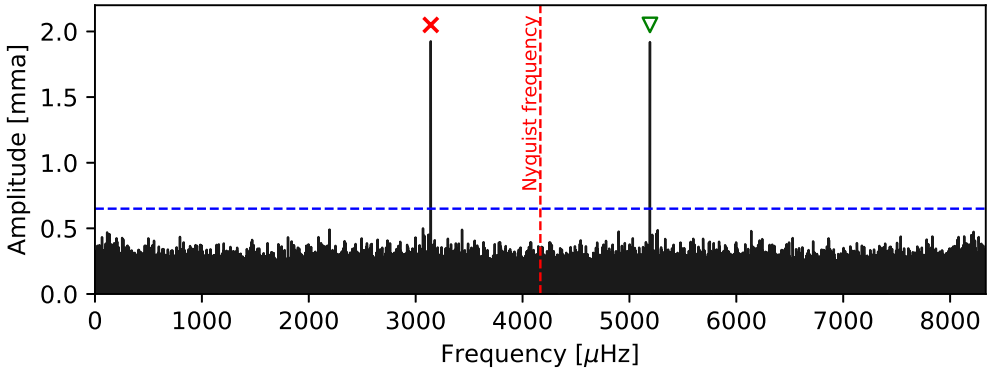

Fig. 9. Fourier transform of TESS light curve of L 19−2 calculated out to twice the Nyquist frequency. The single significant observed signal is reflected across the Nyquist frequency (red dashed line), with the incorrect sub-Nyquist alias marked with a red × and the signal at the intrinsic frequency marked with a green triangle. The blue dashed line indicates the 0.1% FAP level.

3.6. L 19–2

The star L 19−2 (TIC 262872628, G = 13.44 mag, α_{2000} = $14^{h}33^{m}08^{s}$, $\delta_{2000} = -81^{d}20^{m}14^{s}$) was discovered by Hesser et al. (1977).

3.6.1. Ground-based observations

Hesser et al. (1977) found the star to be a relatively simple ZZ Ceti with a pulsation spectrum dominated by two short-period modes with periods of 193 s and 114 s. This star was the target of a Whole Earth Telescope (Nather et al. 1990) campaign in 1995, which revealed L 19−2 to pulsate in at least 10 detectable eigen modes (preliminary analyses are presented in Sullivan 1998; Yeates et al. 2005; Sullivan & Chote 2015). Continued monitoring from Mt John University Observatory was used to measure the secular rate of period change from the cooling (and proper motion) of this white dwarf of $\mathrm{d}P/\mathrm{d}t$ = $(4.0 \pm 0.6)^{-15}$ s s^{-1} (Sullivan & Chote 2015), the third such measurement for a DAV. This value is slightly higher than predicted by asteroseismic models, leading Córsico et al. (2016) to argue that the cooling could be accelerated by the emission of axions. Bradley (2001) also presented asteroseismological constraints on the structure of L 19−2.

3.6.2. TESS observations

The periodogram of the TESS Sector 12 data on L 19−2 reveals a single significant signal at 3141.461 ± 0.013 μHz with an observed amplitude of 1.92 ± 0.11 mma (Table 10). We recognise this as the alias of the dominant mode observed in previous studies of this star, reflected across the Nyquist frequency. We identify the intrinsic signal from this mode in the periodogram computed out to twice the Nyquist frequency, as displayed in Fig. 9. Refining the fit of a sinusoid for this signal to the light curve, we obtain a frequency measurement of 5191.853 ± 0.013 μHz (192.6095 ± 0.0005 s period). The two-minute exposures smooth the light curve, reducing the observed amplitude of this signal to 47% of its intrinsic amplitude. The amplitude measured in shorter exposures would be close to 4 mma, which is comparable to values measured from high speed photometry in the literature, allowing for the difference in observational filters. The second highest amplitude signal previously observed from L 19−2 has a period of 114 s; this is very close to the TESS exposure time,

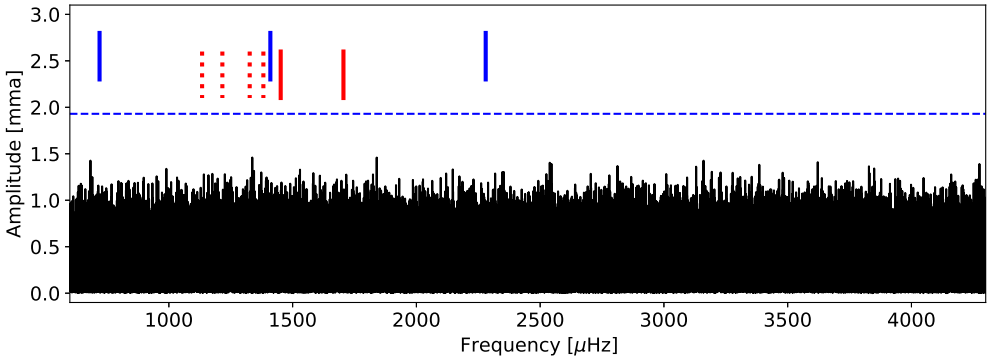

Fig. 10. Fourier transform of Sectors 1–13 of TESS light curve of HE 0532−5605; the blue dashed line indicates the 0.1% FAP level (S/N = 5.24). Vertical red lines mark the frequencies from Fontaine et al. (2003), dashed lines are additional frequencies from that data reported by Castanheira & Kepler (2009), and blue vertical lines (offset upwards) mark those from Kilkenny et al. (2014).

suppressing this signal to well below the periodogram noise floor at 5% its intrinsic amplitude.

3.7. HE 0532−5605

The star HE 0532−5605, (TIC 382303117, G = 15.95 mag, α_{2000} = $05^{h}33^{m}07^{s}$, δ_{2000} = $-56^{d}03^{m}53^{s}$) was discovered in a two-hour duration high S/N photometric observation (Fontaine et al. 2003).

3.7.1. Ground-based observations

The ZZ Ceti star HE 0532−5605 showed two primary periods of oscillation near 688.8 and 586.4 s (1451.8 and 1705.3 μHz), with amplitudes near 8 mma in the observation of Fontaine et al. (2003). Castanheira & Kepler (2009) found this star to be near the red edge of the ZZ Ceti instability strip at $T_{\rm eff}$ = 11 560 K, thus it is expected to have complex and long periodic oscillations generally exceeding 600 s. They identified additional periodicities in the Fontaine et al. (2003) data, ranging from 1100–1950 μHz. The most recent observations of HE 0532−5605 came from Kilkenny et al. (2014), who used the Berkeley Visual Imaging Tube detector to observe HE 0532−5605, for roughly 3000 s with a 0.1 s integration time. They detected periods of 438, 707, and 1380 s (720, 1410, and 2280 μHz, respectively) and indicated that they believed that the periodicity around 1410 μHz may be unstable and related to the peak originally detected by Fontaine et al. (2003).

3.7.2. TESS observations

The star HE 0532−5605, is located near the southern ecliptic pole, and as a result can be observed by TESS for nearly a year. Here, we report on data from all of the 13 available sectors. Each sector was reduced independently, as described earlier, after which point the sectors were combined into a single light curve. The Fourier transform of the entire data set is shown in Fig. 10, and the 0.1% FAP level (S/N = 5.24) lies at 1.93 ppt, which is remarkable given the faintness of the star and the limited aperture of the TESS camera. There are no significant periodicities detected in HE 0532−5605, in the complete data set.

The amplitudes of the modes reported from ground-based studies ranged from 2–8 mma, and were seen in much shorter data sets than the full TESS light curve. Given that the reported periods are in excess of 600 s, and that this is a relatively cool DAV, it is likely that the modes observed from the ground have

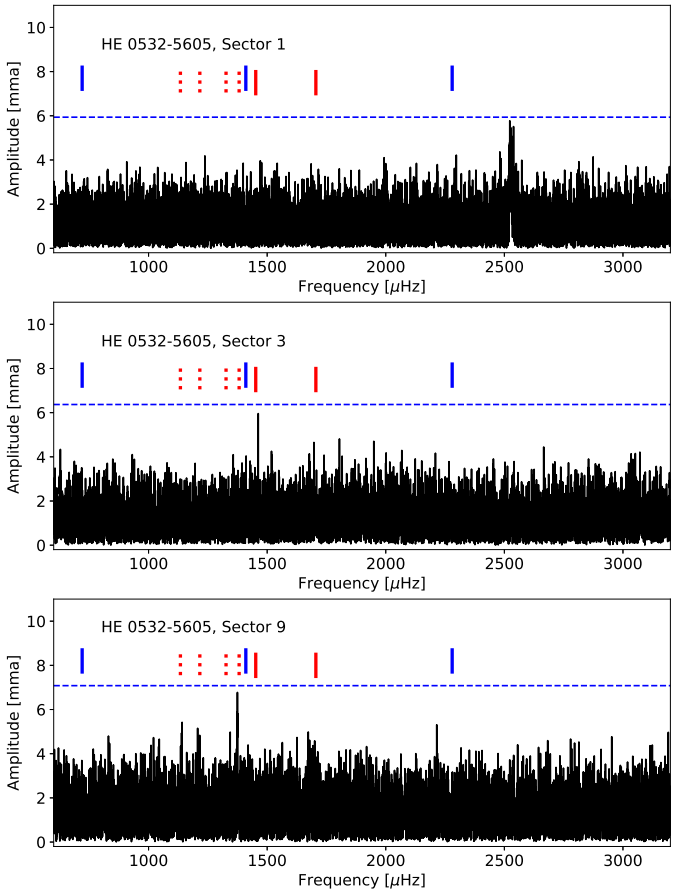

Fig. 11. Fourier transform of three sectors (labelled) of HE 0532−5605 data; the blue dashed line indicates the 0.1% FAP level for each sector. Vertical lines are as in Fig. 10. Other sectors showed no peaks approaching the 0.1% FAP limit.

short lifetimes resulting from changes in phase and amplitude. As we saw in other targets in this study, and as described by Bell et al. (2015), this lack of coherence can reduce the signal amplitude in the Fourier transform if the duration of the observations is much longer than the damping time. Scaling down the expected amplitudes to account for the redder bandwidth of the TESS data can also help explain the failure of these modes to appear in Fig. 10.

To look for shorter-lifetime modes, we examined each sector of the TESS data individually to see if significant periodicities

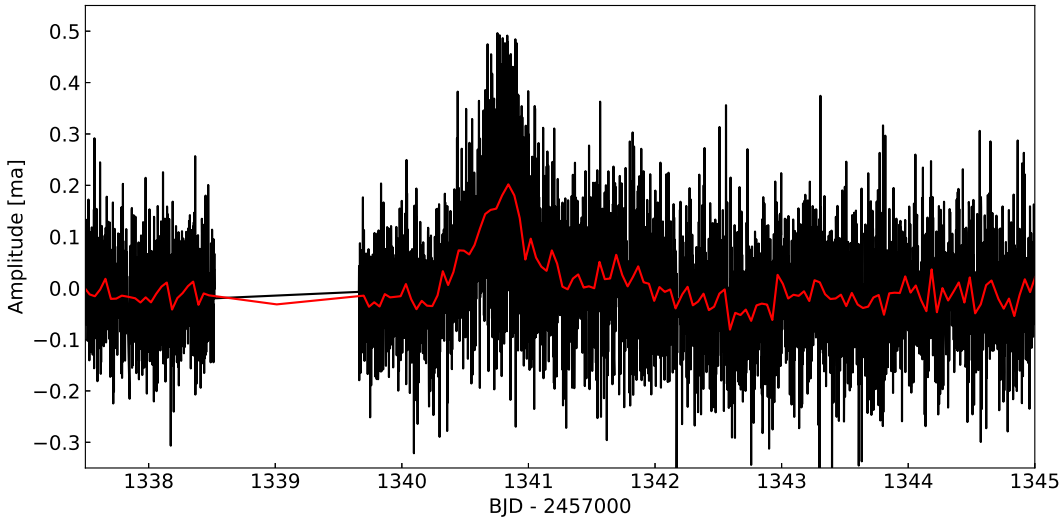

Fig. 12. Light curve of a portion of Sector 1 observations of HE 0532−5605. Red line is binned light curve, with a bin size of 30 points, to show the amplitude and duration of an apparent brightening of 20% for 24 h.

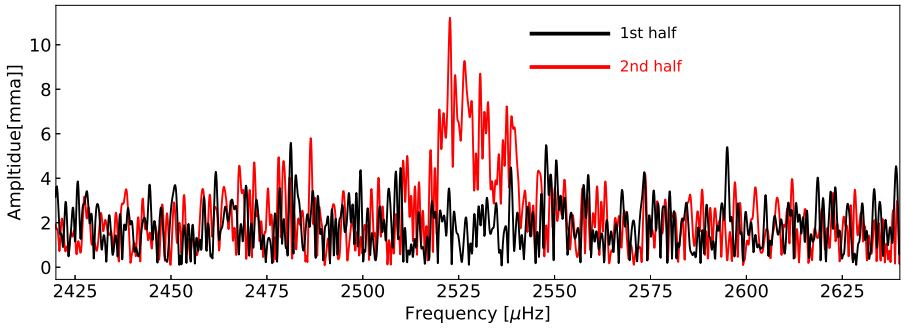

Fig. 13. Fourier transform of Sector 1 data on HE 0532−5605. The black curve is for the first half of Sector 1, and the red curve is for the second half, which contains the candidate burst.

Table 8. Results of the Lorentzian fits to the frequency groups observed in the BPM 30551 data set.

	Frequency [μHz]	Period [s]	Amplitude [mma]	Width [μHz]
f_1	1144.760(150)*	873.546	1.39(03)	8.30(43)
f_2	1204.487(021)*	830.229	3.14(02)	4.41(06)
f_3	1264.164(093)*	789.163	1.83(02)	9.59(26)

Notes. The central frequencies are marked with star symbols (*), as in the case of EC 23487−2424 (Table 5). We also listed the Lorentzian widths for the different fits.

were present. However, since each sector is 1/13 as long as the total run, the noise in the Fourier transform in the individual sectors is nearly three times higher, putting our 0.1% FAP threshold at about 6 mma. No significant periodicities were detected, however, in Sectors 1, 3, and 9, some peaks came close to reaching the 0.1% FAP threshold. We show Fourier transforms of these three sectors in Fig. 11. In Sectors 3 and 9, the highest peaks were close to frequencies reported by Fontaine et al. (2003) and Castanheira & Kepler (2009).

The peak near 2500 μHz in Sector 1 is broad and reminiscent of those seen in the shorter runs on cool DAV stars here (and in Hermes et al. 2017), and in K2 observations of the DAV PG 1149+057 (Hermes et al. 2015). In the latter case, the star in question is a "burster", which shows semiregular increases in brightness coincident with large amplitude pulsations. Close examination of the Sector 1 light curve of HE 0532−5605, suggests that such a burst may have occurred at about BJD 2 458 340. In Fig. 12, we expand the light curve around this interval. For this figure, we did not flatten the light curve, as the flattening process reduced the amplitude of the apparent burst. The possible burst reaches an amplitude of nearly 20%, and the duration is approximately 24 h.

The feature at 2530 μHz in the top panel of Fig. 11 appears to be associated (in time) with the feature at 1341 d (BJD − 2 457 000) in Fig. 12. Figure 13 shows the Fourier transform of the first and second halves of the Sector 1 data on HE 0532−5605. The burst appears soon after the start of the second half of the observation. The feature at 2530 μHz is only present in the second half of the sector as well.

Since this star only showed mildly coherent pulsations during a portion of Sector 1, determining the frequency or frequencies present is a very uncertain task. The FT rose above the significance threshold between approximately 2520 and 2550 μHz. We fit a Lorentzian envelope to the strongest part of this range, and thus estimate the frequency for this mode at approximately 2527 μHz.

It appears, therefore, that HE 0532−5605, may be a bursting, pulsating DA white dwarf. The duration and amplitude of

Table 9. Complete list of frequencies, periods, and amplitudes derived from the MCT 0145−2211 data set.

Frequency [μHz]	Period [s]	Amplitude [mma]
955.854(044)	1046.185	3.68(53)
1253.099(045)	798.021	3.63(1.89)
1257.085(063)	795.491	5.29(53)
1257.462(052)	795.252	6.40(88)
1297.472(039)	770.730	4.13(62)
1305.221(045)	766.154	3.72(55)
1306.979(033)	765.123	5.21(89)
1308.725(053)	764.103	3.18(55)
1317.983(046)	758.735	3.52(1.90)
2213.161(046)	451.842	5.58(63)
2213.695(052)	451.733	8.13(54)
2214.635(062)	451.542	11.36(54)
2214.985(055)	451.470	8.35(53)
2407.200(015)	415.420	10.90(53)

Table 10. Frequency derived from the L 19−2 data set.

Frequency [μHz]	Period [s]	Ampl. [mma]
5191.853(013)	192.610	1.92(11)

the burst, and the increased pulsation amplitude during the burst, has been seen in other stars. However, most of the bursting white dwarfs recur on an irregular basis, but roughly every eight days or so. No other clear bursts have been seen in the TESS data over 13 sectors, though it is possible that the nearly significant features in Sectors 3 and 9 may reflect smaller bursts that aren't apparent in the relatively low S/N data from this faint star. Also, the periodicity present during the burst is at a relatively short period (395 s, or 2530 μHz). The star HE 0532−5605, merits monitoring with larger instruments to confirm its possible membership in the rare class of bursting, pulsating DA white dwarfs.

3.8. HS 0507+0434B

The star HS 0507+0434B (TIC 455094688, $G = 15.40$ mag, $\alpha_{2000} = 05^{h}10^{m}14^{s}$, $\delta_{2000} = +04^{d}38^{m}55^{s}$) was discovered to be a member of the ZZ Ceti class by Jordan et al. (1998).

3.8.1. Ground-based observations

The observations of Jordan et al. (1998) showed that the star's light variations can be described with three or four independent modes at 278.4, 355.1, 445.2, and 558.7 s, and a large number of combination terms, with 18 frequencies altogether. Further observations revealed that at some frequencies there are actually rotationally split triplets. Handler et al. (2002) detected ten independent frequencies consisting of three triplets and a singlet frequency, and also a large number of combination frequencies, while Kotak et al. (2002) detected two doublets and three additional modes besides the combination terms. Castanheira & Kepler (2009) listed four modes for their asteroseismic fit, while the latest time-series photometric observations on HS 0507+0434B were presented by Fu et al. (2013). They derived 18 independent pulsation frequencies consisting of five triplets, a doublet, and a singlet frequency besides the combination terms.

Table 11. Six-frequency solution of the HS 0507+0434B data set.

	Frequency [μHz]	Period [s]	Amplitude [mma]
f_1	1680.072(32)	595.213	5.42(71)
f_2^{-1}	2242.401(13)	445.950	13.08(71)
f_2^{+1}	2248.078(28)	444.824	6.07(71)
f_3^{-1}	2810.935(12)	355.754	14.66(72)
(f_3^{-0})	2814.347(52)	355.322	3.29(72)
f_3^{+1}	2817.615(18)	354.910	9.33(72)

Notes. The errors are formal uncertainties calculated by FAMIAS. In the case of the rotationally split frequencies, we mark the azimuthal order values, based on the results of the subsequent observations.

3.8.2. TESS observations

Contrary to the rich frequency spectrum observed, for example, by Fu et al. (2013), we only detected five peaks in the TESS data set of HS 0507+0434B above the significance level. Table 11 lists the frequencies, periods, and amplitudes of these peaks. The 1680.072 μHz frequency represents a new mode not observed before, while the other four peaks are side components of formerly detected triplets. No combination frequencies could be derived by the TESS data, however, we have to take into account the amplitude suppression factor of the two-minute exposures, especially in the case of peaks expected to emerge with low amplitudes. We note that we listed an additional peak in Table 11 in parentheses. This represents the central component of the ~2810 μHz triplet, however, this peak is under our significance threshold ($S/N = 3.7$).

The f_2 and f_3 frequencies are found to be stable during the time-span of the TESS observations, as these frequency domains can be pre-whitened with the doublet frequencies alone, and no further closely spaced frequencies emerged as in, for example, EC 23487−2424. Figure 14 shows the original and the pre-whitened Fourier transforms, respectively.

Considering the influence of the companion HS 0507+0434A (TIC 455094685) on the frequency determination of HS 0507+0434B, we found that TESS cannot separate individual signals from these two objects since the separation between the two stars (~15 arcsec) is smaller than the plate scale of the TESS detector (21 arcsec px^{-1}). However, investigating the amplitudes of the signals originating from the two sources, we found that at the position of HS 0507+0434B, the measured amplitudes are a factor of 4.02 ± 0.04 (error of the mean) larger than at the position of HS 0507+0434A, so they must come from component B. Another argument that the frequencies detected belong to HS 0507+0434B, is that there are ground-based studies which clearly resolve both components, including the paper of Handler et al. (2002), where the authors studied the variability of HS 0507+0434B, using HS 0507+0434A as well as other stars for comparison.

3.9. ZZ Ceti stars not seen to vary in the TESS data

TESS targeted additional previously known, bright ZZ Ceti variables in the southern hemisphere that did not exhibit significant pulsation signals in the TESS data, namely MCT 2148−2911,

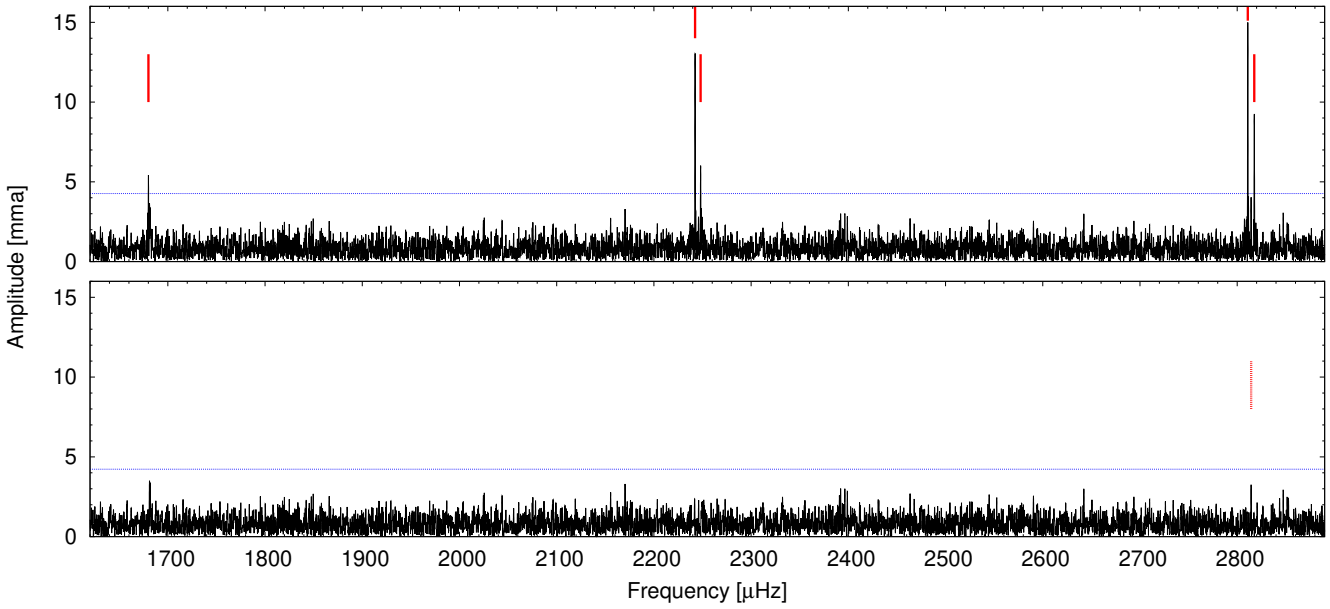

Fig. 14. Fourier transform of light curve of HS 0507+0434B before (*upper panel*) and after (*lower panel*) pre-whitening with the five significant frequencies. Red dashed lines mark the frequencies listed in Table 11, while the blue dashed lines represent the 0.1% FAP levels (S/N = 4.73).

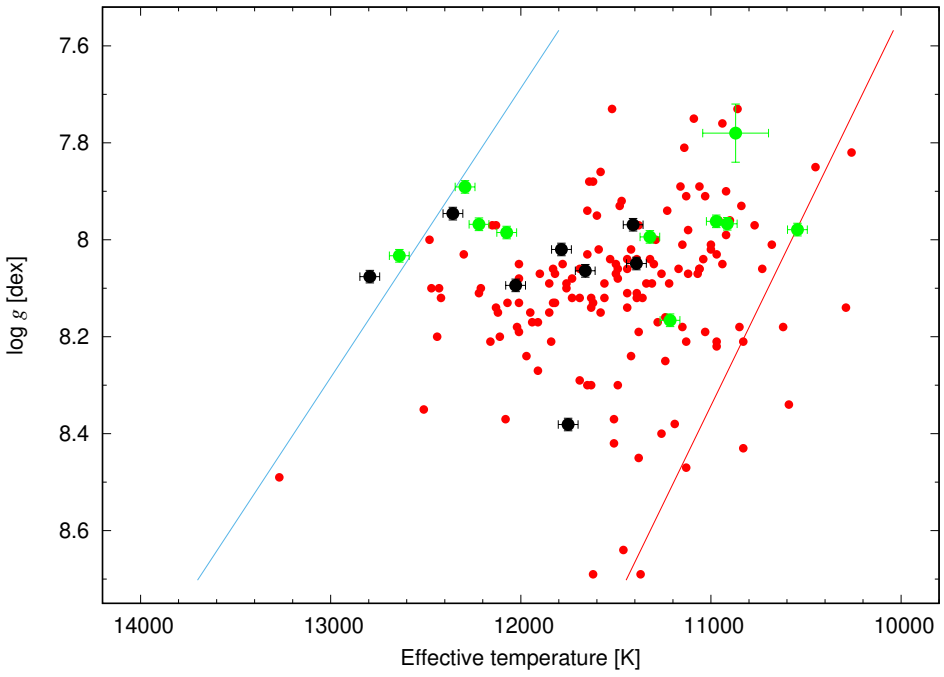

Fig. 15. Known ZZ Ceti stars (red filled dots, atmospheric parameters from Bognár & Sódor 2016), and DAVs observed by TESS during the survey measurements of the southern ecliptic hemisphere (sectors 1–13) in the $T_{\rm eff}$ − $\log g$ diagram. Black and green dots mark the stars found to be variable and not seen to vary by the TESS measurements, respectively. Their atmospheric parameters were derived by Fuchs (2017), except in the case of KUV 03442+0719, where we used the values presented in Bognár & Sódor (2016). Blue and red lines denote the hot and cool boundaries of the instability strip, according to Tremblay et al. (2015).

HE 0031−5525, EC 00497−4723, MCT 0016−2553, WD 0108−001, HS 0235+0655, KUV 03442+0719, WD J0925+0509, HS 1013+0321, and EC 11266−2217. For completeness, we report on these ten stars in Appendix B, comparing the upper-limit detection thresholds of the TESS data to pulsation amplitudes reported in the literature.

4. Summary and conclusions

We presented the frequency analysis of 18 previously known ZZ Ceti stars observed by the TESS space telescope during the survey observation of the southern ecliptic hemisphere (Sectors 1–13). We compared our results to those from previous ground-based observing campaigns. Eight out of 18 of our targets show at least marginal evidence of pulsations that we were able to characterise, with at least 40 statistically significant (FAP < 0.1%) pulsation detections in total. From ∼month-long TESS light curves with very high duty cycles, we measured pulsation frequencies to $\lesssim$0.1 μHz precision. These are eigen frequencies of these white dwarf stars, and they can be compared to stellar models to infer the interior conditions of these compact pulsators. A follow-up paper from TASC WG#8 is planned (Romero et al., in prep.), and we will use different sets of models to interpret the precision measurements reported here.

Figure 15 shows the ZZ Ceti instability strip with known ZZ Ceti stars (atmospheric parameters are from Bognár & Sódor 2016), together with all the 18 objects studied in this paper. The corresponding atmospheric parameters from the literature are listed in Table 12 for the 18 targets (Fuchs 2017). The $T_{\rm eff}$ and $\log g$ values were determined by the use of the ML2/α = 0.8

Table 12. Atmospheric parameters of the ZZ Ceti stars observed by TESS during the survey measurements of the southern ecliptic hemisphere (Sectors 1–13).

Object	$T_{\rm eff}$ [K]	log g [dex]
Ross 548	12 357	7.946
EC 23487−2424	11 409	7.969
BPM 31594	11 786	8.020
BPM 30551	11 392	8.049
MCT 0145−2211	11 661	8.064
L 19−2	12 794	8.076
HE 0532−5605	11 751	8.381
HS 0507+0434B	12 027	8.094
MCT 2148−2911	12 220	7.968
EC 00497−4723	11 321	7.994
EC 11266−2217	12 074	7.985
MCT 0016−2553	10 972	7.962
HS 1013+0321	12 639	8.033
HE 0031−5525	12 293	7.891
WD J0925+0509	11 215	8.166
WD 0108−001	10 545	7.979
HS 0235+0655	10 914	7.967
KUV 03442+0719	10 870	7.78

Notes. The $T_{\rm eff}$ and log$g$ values are from Fuchs (2017), except for KUV 03442+0719, where we used the values listed in Bognár & Sódor (2016). The external uncertainties for the observations presented by Fuchs (2017) are 52 K in $T_{\rm eff}$ and 0.013 dex in log g, respectively, while 173 K and 0.06 dex for KUV 03442+0719, as given by Gianninas et al. (2011).

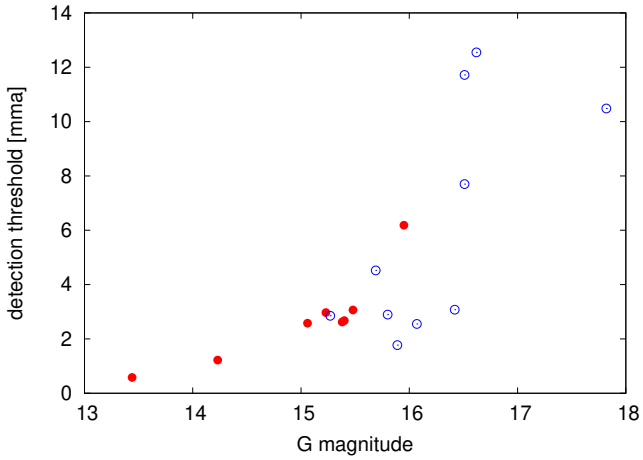

Fig. 16. Pulsation-detection performance of TESS. Stars confirmed (red dots) or not seen to vary (blue circles) by the TESS observations in the G magnitude-detection threshold diagram, where the detection threshold is defined as $0.1\%\mathrm{FAP} \times \sqrt{\mathrm{CROWDSAP}} \times \sqrt{\mathrm{number\ of\ sectors}}$.

version of the mixing-length theory, and corrected according to the findings of Tremblay et al. (2013) based on radiation-hydrodynamics 3D simulations of convective DA stellar atmospheres.

We demonstrated the difference between the TESS amplitudes and those detected in the ground-based measurements through the case of Ross 548. We have to take several different effects into account. Firstly, TESS observes in a redder band pass than typical ground-based observations, which results in lower pulsation amplitudes (see Eq. (1)). Secondly, the relatively large pixel size of TESS often causes contamination, and hence signal-to-noise suppression. Thirdly, the 120 s exposure times of the TESS observations smear out the short-period signals of the ZZ Ceti stars. And finally, phase and/or amplitude variations on timescales shorter than the month-long TESS light curves reduce the pulsation amplitudes by distributing power across multiple frequency bins. These effects explain why we did not detect pulsations in ten low-amplitude pulsators, and why there are missing frequencies compared to the ground-based results in some of the TESS variables.

The detection threshold corresponding to an uncontaminated target in a single sector is defined as $0.1\%\,\mathrm{FAP} \times \sqrt{\mathrm{CROWDSAP}} \times \sqrt{\mathrm{number\ of\ sectors}}$ and is shown in Fig. 16. The plot demonstrates the pulsation-detection performance of TESS. This threshold obviously depends on the magnitude of the ZZ Ceti star. The eight stars with confirmed pulsations have $G < 15.5$ mag (except for HE 0532−5605). The brightest of the stars with unconfirmed pulsations is $G = 15.3$ mag, and most are fainter than $G = 15.8$ mag. There is, however, significant scatter in the calculated threshold at a given brightness, especially at targets fainter than 15.5 mag, possibly due to instrumental effects.

In spite of the difficulties, we were able to detect new frequencies for five stars (EC 23487−2424, BPM 31594, BPM 30551, MCT 0145−2211, HS 0507+0434B). We found that HE 0532−5605 may be a new outbursting ZZ Ceti star. We also found possible amplitude or phase variations during the TESS observations, which resulted in the emergence of groups of peaks in the data set of EC 23487−2424, BPM 30551, and MCT 0145−2211. We fit Lorentzians to these frequency groups to approximate pulsation frequency values. Such behaviour in these stars had not been identified from the ground before.

Another thing we can learn from the TESS measurements is that we have to be cautious with the interpretation of the frequencies considering the Nyquist-limit of the 120 s exposures ($\approx$4167 μHz). In the case of the peaks close to the Nyquist frequency, we have to take into account the possibility that these are intrinsically above the Nyquist-limit. The barycentric correction applied to the observation timings makes the data deviate from strict equidistancy that, in turn, lifts Nyquist-degeneracy, that is, the pseudo-Nyquist alias will have lower amplitude in the Fourier spectrum than the real frequency peak (Murphy et al. 2013). However, in the month-long TESS observations, this effect is far too weak for safe discrimination. We find that the amplitudes across $n \times$ Nyquist behave differently depending on a star. In some stars, the amplitudes are the highest in the sub-Nyquist region, getting lower with increasing frequency, however, sometimes we see that the amplitudes of the signals in question are changing significantly up and down, while being higher in the super-Nyquist region across many times the Nyquist frequency. Some of this behavior could be caused by intrinsic variations of the pulsation signals.

Despite these difficulties, TESS observations of ZZ Ceti stars proved that measurements of bright DAVs allow us to detect the signs of short-term amplitude or phase variations, and also derive new pulsation modes with high precision thanks to the (almost) continuous, homogeneous and high-quality data. However, the value of 20 s cadence observations is also obvious. The two-minute cadence induces a significant decrease of amplitudes, which is largely responsible for the nondetection of pulsations

in several targets. Offering 20 s cadence mode observations for short-period compact pulsators in the extended mission could infer a breakthrough in the study of these kinds of variables.

Acknowledgements. The authors thank the anonymous referee for the constructive comments and recommendations on the manuscript. We also thank the comments of Kosmas Gazeas (National and Kapodistrian University of Athens). This paper includes data collected with the TESS mission, obtained from the MAST data archive at the Space Telescope Science Institute (STScI). Funding for the TESS mission is provided by the NASA Explorer Program. STScI is operated by the Association of Universities for Research in Astronomy, Inc., under NASA contract NAS 5–26555. Support for this work was provided by NASA through the TESS Guest Investigator program through grant 80NSSC19K0378. ZsB acknowledges the support provided from the National Research, Development and Innovation Fund of Hungary, financed under the PD_{17} funding scheme, project no. PD-123910. This project has been supported by the Lendület Program of the Hungarian Academy of Sciences, project No. LP2018-7/2019. KJB is supported by the National Science Foundation under Award No. AST-1903828. ASB gratefully acknowledges financial support from the Polish National Science Center under project No. UMO-2017/26/E/ST9/00703. GH acknowledges financial support by the Polish NCN grant 2015/18/A/ST9/00578. RR acknowledges funding by the German Science foundation (DFG) through grants HE1356/71-1 and IR190/1-1. WZ acknowledges the support from the Beijing Natural Science Foundation (No. 1194023) and the National Natural Science Foundation of China (NSFC) through the grant 11903005.

References

Aerts, C., Christensen-Dalsgaard, J., & Kurtz, D. W. 2010, Asteroseismology (Dordrecht: Springer)
Althaus, L. G., Córsico, A. H., Isern, J., & García-Berro, E. 2010, A&ARv, 18, 471
Baran, A. S., Reed, M. D., Stello, D., et al. 2012, MNRAS, 424, 2686
Barentsen, G., Hedges, C. L., De Mirand a Cardoso, J. V., et al. 2019, Am. Astron. Soc. Meet. Abstr., 233, 109.08
Bell, K. J., Hermes, J. J., Bischoff-Kim, A., et al. 2015, ApJ, 809, 14
Bell, K. J., Hermes, J. J., Montgomery, M. H., et al. 2016, ApJ, 829, 82
Bell, K. J., Hermes, J. J., Montgomery, M. H., et al. 2017a, ASP Conf. Ser., 509, 303
Bell, K. J., Hermes, J. J., Vanderbosch, Z., et al. 2017b, ApJ, 851, 24
Bell, K. J., Córsico, A. H., Bischoff-Kim, A., et al. 2019, A&A, 632, A42
Bognár, Z., & Sódor, A. 2016, Inf. Bull. Var. Stars, 6184, 1
Bradley, P. A. 2001, ApJ, 552, 326
Castanheira, B. G., & Kepler, S. O. 2009, MNRAS, 396, 1709
Castanheira, B. G., Kepler, S. O., Mullally, F., et al. 2006, A&A, 450, 227
Castanheira, B. G., Kepler, S. O., Kleinman, S. J., Nitta, A., & Fraga, L. 2010, MNRAS, 405, 2561
Charpinet, S., Brassard, P., Fontaine, G., et al. 2019, A&A, 632, A90
Córsico, A. H., Romero, A. D., Althaus, L. R. G., et al. 2016, JCAP, 2016, 036
Córsico, A. H., Althaus, L. G., Miller Bertolami, M. M., & Kepler, S. O. 2019, A&ARv, 27, 7
Fontaine, G., & Brassard, P. 2008, PASP, 120, 1043
Fontaine, G., Bergeron, P., Billères, M., & Charpinet, S. 2003, ApJ, 591, 1184
Fu, J. N., Dolez, N., Vauclair, G., et al. 2013, MNRAS, 429, 1585
Fuchs, J. T. 2017, PhD Thesis, The University of North Carolina at Chapel Hill
Gaia Collaboration 2018, VizieR Online Data Catalog: I/345
Gentile Fusillo, N. P., Tremblay, P.-E., Gänsicke, B. T., et al. 2019, MNRAS, 482, 4570
Giammichele, N., Fontaine, G., Bergeron, P., et al. 2015, ApJ, 815, 56
Gianninas, A., Bergeron, P., & Fontaine, G. 2006, AJ, 132, 831
Gianninas, A., Bergeron, P., & Ruiz, M. T. 2011, ApJ, 743, 138
Handler, G., Romero-Colmenero, E., & Montgomery, M. H. 2002, MNRAS, 335, 399
Hermes, J. J., Montgomery, M. H., Bell, K. J., et al. 2015, ApJ, 810, L5
Hermes, J. J., Gänsicke, B. T., Kawaler, S. D., et al. 2017, ApJS, 232, 23
Hesser, J. E., Lasker, B. M., & Neupert, H. E. 1976, ApJ, 209, 853
Hesser, J. E., Lasker, B. M., & Neupert, H. E. 1977, ApJ, 215, L75
Jenkins, J. M., Twicken, J. D., McCauliff, S., et al. 2016, Proc. SPIE, 9913, 99133E
Jordan, S., Koester, D., Vauclair, G., et al. 1998, A&A, 330, 277
Kawaler, S. D., Bond, H. E., Sherbert, L. E., & Watson, T. K. 1994, AJ, 107, 298
Kilkenny, D., Welsh, B. Y., Koen, C., Gulbis, A. A. S., & Kotze, M. M. 2014, MNRAS, 437, 1836
Koch, D. G., Borucki, W. J., Basri, G., et al. 2010, ApJ, 713, L79
Kotak, R., van Kerkwijk, M. H., & Clemens, J. C. 2002, A&A, 388, 219
Lasker, B. M., & Hesser, J. E. 1971, ApJ, 163, L89
McGraw, J. T. 1976, ApJ, 210, L35
Montgomery, M. H., Provencal, J. L., Kanaan, A., et al. 2010, ApJ, 716, 84
Mukadam, A. S., Mullally, F., Nather, R. E., et al. 2004, ApJ, 607, 982
Mukadam, A. S., Bischoff-Kim, A., Fraser, O., et al. 2013, ApJ, 771, 17
Mullally, F., Winget, D. E., Degennaro, S., et al. 2008, ApJ, 676, 573
Murphy, S. J., Shibahashi, H., & Kurtz, D. W. 2013, MNRAS, 430, 2986
Nather, R. E., Winget, D. E., Clemens, J. C., Hansen, C. J., & Hine, B. P. 1990, ApJ, 361, 309
Odonoghue, D. 1986, MNRAS, 220, 19P
O'Donoghue, D., Warner, B., & Cropper, M. 1992, MNRAS, 258, 415
Pyrzas, S., Gänsicke, B. T., Hermes, J. J., et al. 2015, MNRAS, 447, 691
Ricker, G. R., Winn, J. N., Vanderspek, R., et al. 2015, J. Astron. Telesc. Instrum. Syst., 1, 014003
Stobie, R. S., Chen, A., O'Donoghue, D., & Kilkenny, D. 1993, MNRAS, 263, L13
Stobie, R. S., Kilkenny, D., Koen, C., & O'Donoghue, D. 1997, in The Third Conference on Faint Blue Stars, eds. A. G. D. Philip, J. Liebert, R. Saffer, & D. S. Hayes, 497
Sullivan, D. J. 1998, Balt. Astron., 7, 159
Sullivan, D. J., & Chote, P. 2015, ASP Conf. Ser., 493, 199
Thompson, S. E., Clemens, J. C., & Koester, D. 2005, ASP Conf. Ser., 334, 471
Tremblay, P. E., Ludwig, H. G., Steffen, M., & Freytag, B. 2013, A&A, 559, A104
Tremblay, P. E., Gianninas, A., Kilic, M., et al. 2015, ApJ, 809, 148
Twicken, J. D., Chandrasekaran, H., Jenkins, J. M., et al. 2010, Proc. SPIE, 7740, 77401U
Voss, B., Koester, D., Østensen, R., et al. 2006, A&A, 450, 1061
Voss, B., Koester, D., Østensen, R., et al. 2007, ASP Conf. Ser., 372, 583
Winget, D. E., & Kepler, S. O. 2008, ARA&A, 46, 157
Yeates, C. M., Clemens, J. C., Thompson, S. E., & Mullally, F. 2005, ApJ, 635, 1239
Zima, W. 2008, Commun. Asteroseismol., 155, 17
Zong, W., Charpinet, S., Vauclair, G., Giammichele, N., & Van Grootel, V. 2016, A&A, 585, A22

Appendix A: TESS light curves of stars that are confirmed to vary

TESS light curves of stars that are confirmed to vary, see Fig. A.1.

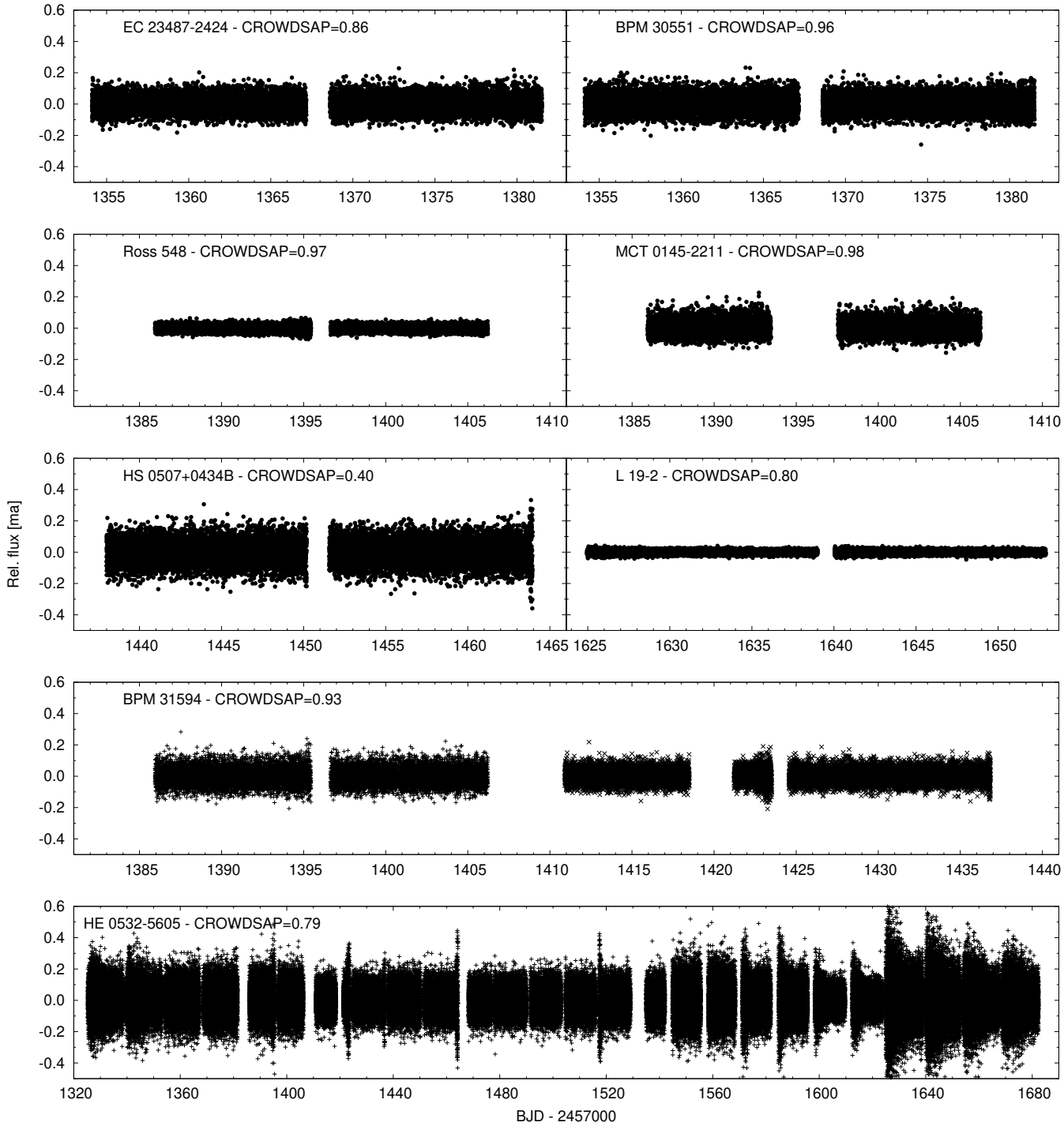

Fig. A.1. Reduced TESS light curves of eight ZZ Ceti stars found to be variables by the TESS data. We note that the light curve of HE 0532−5605 is on a different scale, and represents 13 sectors of data. We also denoted the values of the CROWDSAP keywords listed in the fits headers, which represent the ratio of the target flux to the total flux in the aperture.

Appendix B: ZZ Ceti stars not seen to vary

Figure B.1 shows the TESS light curves of the stars not seen to vary, while Fig. B.2 displays the Fourier transforms of the light curves of each of these stars along with the 0.1% FAP significance thresholds.

MCT 2148−2911 (TIC 053851007, $G = 16.07$ mag, $\alpha_{2000} = 21^{h}51^{m}40^{s}$, $\delta_{2000} = -28^{d}56^{m}53^{s}$), also referred to as WD 2148−291, was discovered to be a ZZ Ceti variable by Gianninas et al. (2006). From a one-hour light curve obtained in the *B*-band, they detected a single short-period signal of 260.8 s with an amplitude of 12.6 mma. We identify no signals in the periodogram of the TESS Sector 1 light curve that exceed the 0.1% FAP significance threshold of 6.19 mma, and specifically see no compelling peaks at the frequency measured by Gianninas et al. (2006). This is not surprising, considering that the two-minute TESS exposures reduce the measured amplitude of a signal with this period to 69% of its intrinsic amplitude, and the effect of observing in a redder band pass reduces the amplitude again by a comparable factor (Sect. 3.1). Worse still, 83% of the flux in the TESS aperture comes from other blended sources (CROWDSAP = 0.17), causing the significance threshold for this target to be 2.8 times higher than we would expect for an unblended source of the same magnitude.

HE 0031−5525 (TIC 281594636, $G = 15.80$ mag, $\alpha_{2000} = 00^{h}33^{m}36^{s}$, $\delta_{2000} = -55^{d}08^{m}39^{s}$) has a relatively low surface gravity for a ZZ Ceti variable, with $\log g = 7.65 \pm 0.02$ determined by Castanheira et al. (2006) from fitting hydrogen atmosphere models to the Balmer lines observed in its spectrum from the Hamburg ESO survey. However, *Gaia* DR2 observations are consistent with a higher surface gravity, $\log g = 7.92 \pm 0.02$ (Gentile Fusillo et al. 2019). From five nights of time series photometry from the 1.6 m and 0.6 m telescopes at Observatório Pico dos Dias, LNA, in Brazil, they detected three pulsation modes dominated by a 4.8 mma signal with a period of 276.9 s. This star was observed by TESS in Sector 2 as TIC 281594636, but with a significance threshold of 5.47 mma (particularly high for a target of this magnitude due to blending of nearby sources), we do not detect any pulsation signals from this data set.

EC 00497−4723 (TIC 101916028, $G = 16.51$ mag, $\alpha_{2000} = 00^{h}52^{m}01^{s}$, $\delta_{2000} = -47^{d}07^{m}09^{s}$) was reported as a ZZ Ceti pulsator in conference proceedings by Stobie et al. (1997) based on multiple nights of both photoelectric and CCD observations. A detailed analysis of these data is not presented, though the dominant pulsations in the 500–1000 s range appear to vary in amplitude between roughly 10–20 mma depending on the night. This star was observed by TESS in Sector 2, with no significant signals detected above our 8.35 mma threshold. The rough daytimescale variations in pulsation amplitudes that were observed from the ground could significantly reduce their amplitudes measured in the TESS periodogram compared to the average instantaneous pulsation amplitudes as power is distributed across multiple frequency bins.

MCT 0016−2553 (TIC 246821917, $G = 15.89$ mag, $\alpha_{2000} = 00^{h}18^{m}45^{s}$, $\delta_{2000} = -25^{d}36^{m}43^{s}$) was also discovered to pulsate by Gianninas et al. (2006). They detected a single pulsation signal with a 1152.4 s period and an amplitude of 8.1 mma in white light. We do not detect any significant signals in the TESS Sector 2 light curve of MCT 0016−2553 to a threshold of 4.92 mma, and we lose a lot of sensitivity because of blending of nearby sources within the TESS aperture (CROWDSAP = 0.13).

WD 0108−001 (TIC 336891566, $G = 17.82$ mag, $\alpha_{2000} = 01^{h}11^{m}24^{s}$, $\delta_{2000} = +00^{d}09^{m}35^{s}$) was reported as SDSS J0111+0009 to be a ZZ Ceti variable in a wide binary system with an M dwarf companion by Pyrzas et al. (2015). This target happened to fall within the field of K2 Campaign 8 and was observed for 78.72 days with a 1 min cadence. Hermes et al. (2017) detected 14 frequencies associated with seven independent pulsation modes from this data set, though the largest amplitude measured from the K2 light curve reached only 3.88 mma: well below the noise level of the TESS Sector 3 periodogram (0.1% FAP threshold is 10.93 mma).

HS 0235+0655 (TIC 365247111, $G = 16.51$ mag, $\alpha_{2000} = 02^{h}38^{m}33^{s}$, $\delta_{2000} = +07^{d}08^{m}09^{s}$) was discovered to pulsate by Voss et al. (2007). They report a single main periodicity of 1283.7 s with an amplitude of 4.21 mma, though the 1.2 h light curve segment they display exhibits the characteristic amplitude modulation caused by beating of closely spaced modes. The periodogram of the TESS Sector 4 light curve achieved a very low signal-to-noise ratio, with a 0.1% FAP threshold of 12.42 mma.

KUV 03442+0719 (TIC 468887063, $G = 16.62$ mag, $\alpha_{2000} = 03^{h}46^{m}51^{s}$, $\delta_{2000} = +07^{d}28^{m}03^{s}$) was discovered to pulsate with an amplitude of 7.6 mma at a dominant period of 1384.9 s by Gianninas et al. (2006). Curiously, Voss et al. (2007) did not detect any pulsations from this star to a limit of 2 mma. Unsurprisingly, no signals exceed the 16.62 mma detection threshold of the TESS Sector 5 data.

WD J0925+0509 (TIC 290653324, $G = 15.27$ mag, $\alpha_{2000} = 09^{h}25^{m}12^{s}$, $\delta_{2000} = +05^{d}09^{m}33^{s}$) found to be a massive white dwarf of $0.87 \pm 0.01\,M_{\odot}$ that was discovered to pulsate by Castanheira et al. (2010), who detected two signals with periods 1127.14 and 1264.29 s with low amplitudes of 3.17 and 3.05 mma, respectively. However, *Gaia* DR2 observations suggest a moderate mass of $M_{*} = 0.74 \pm 0.01\,M_{\odot}$ (Gentile Fusillo et al. 2019). The TESS Sector 8 data are only sensitive to signals that exceed a 3.81 mma threshold, of which we find none.

HS 1013+0321 (TIC 277747736, $G = 15.69$ mag, $\alpha_{2000} = 10^{h}15^{m}48^{s}$, $\delta_{2000} = +03^{d}06^{m}48^{s}$) is a ZZ Ceti near the hot edge of the instability strip that was detected to pulsate with three modes of periods (amplitudes) 270.0 s (8.4 mma), 255.7 s (7.3 mma), and 194.7 s (5.8 mma) by Mukadam et al. (2004). Continued monitoring of this star by Mullally et al. (2008) refined the measurement of the second period to 254.918450 ± 0.000006 s, and constrained the rate of change of the period to $\dot{P} = (7.2 \pm 3.6) \times 10^{13}$ s s^{-1}. The observable amplitudes of these short period modes would all be significantly decreased by TESS's two-minute exposures, and none appear to exceed the significance threshold of 4.59 mma from the Sector 8 light curve.

EC 11266−2217 (TIC 219442838, $G = 16.42$ mag, $\alpha_{2000} = 11^{h}29^{m}12^{s}$, $\delta_{2000} = -22^{d}33^{m}44^{s}$) was discovered to exhibit at least four pulsation signals between 215 and 403 s by Voss et al. (2006), with the highest peak reaching an amplitude of 7 mma. The TESS Sector 9 data do not reveal any signals to exceed a 5.20 mma detection limit. The light curve does exhibit two moments of significant brightness enhancement during days 2 458 545 and 2 458 548 BJD, the first reaching as high as 2.8 times the mean flux level in the processed light curve (Fig. B.1). These are caused by stellar flares of the nearby M-dwarf star that contributes most of the flux to the TESS photometric aperture (the mean contaminating flux level of 65% was subtracted from the light curve by the PDC pipeline; Twicken et al. 2010). Astrometry from *Gaia* DR2 indicates that this M dwarf (`source_id` 3541237717085786880) is a common-proper-motion companion to the ZZ Ceti variable (`source_id` 3541237717085787008).

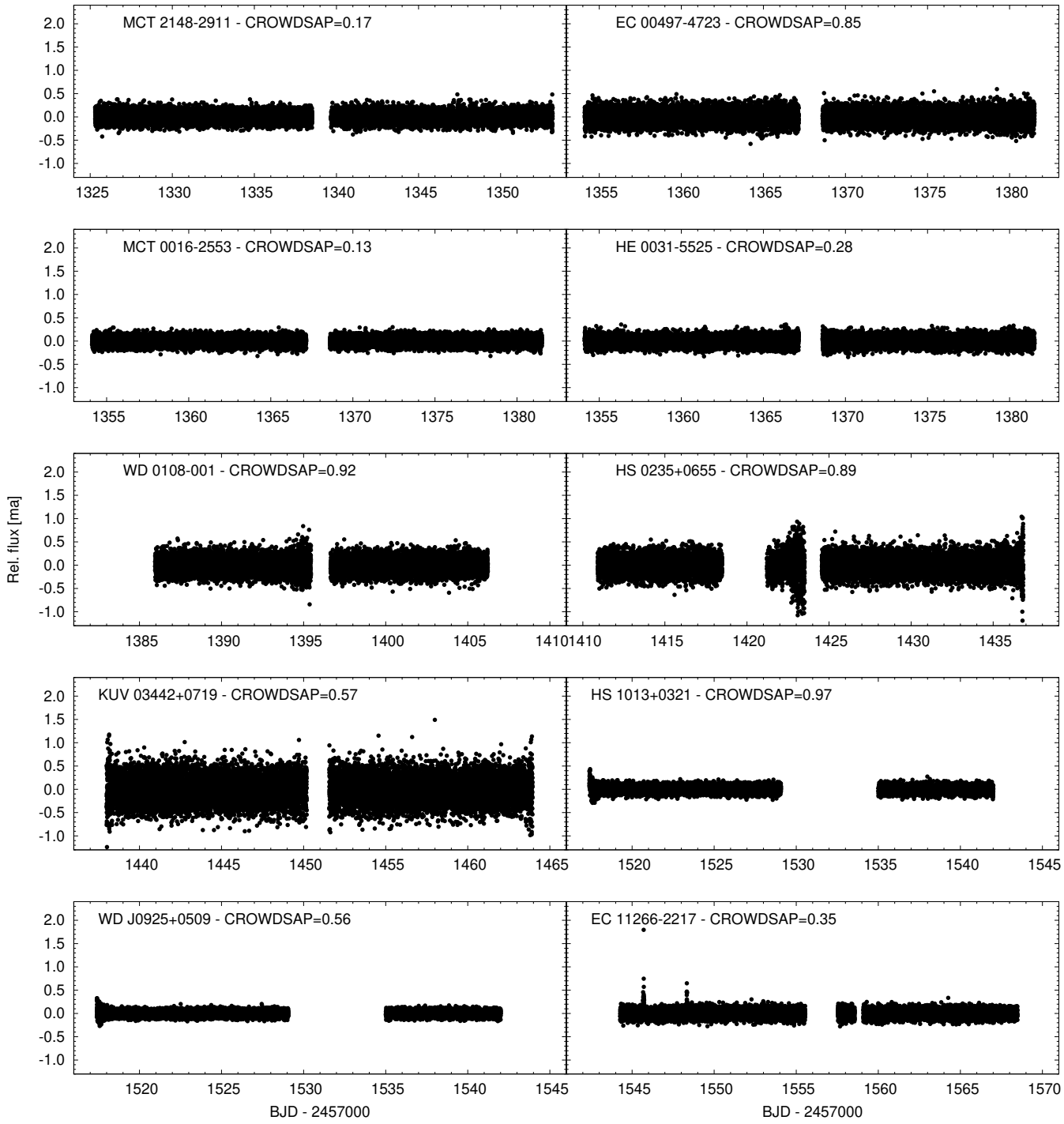

Fig. B.1. Reduced TESS light curves of ZZ Ceti stars not seen to vary.

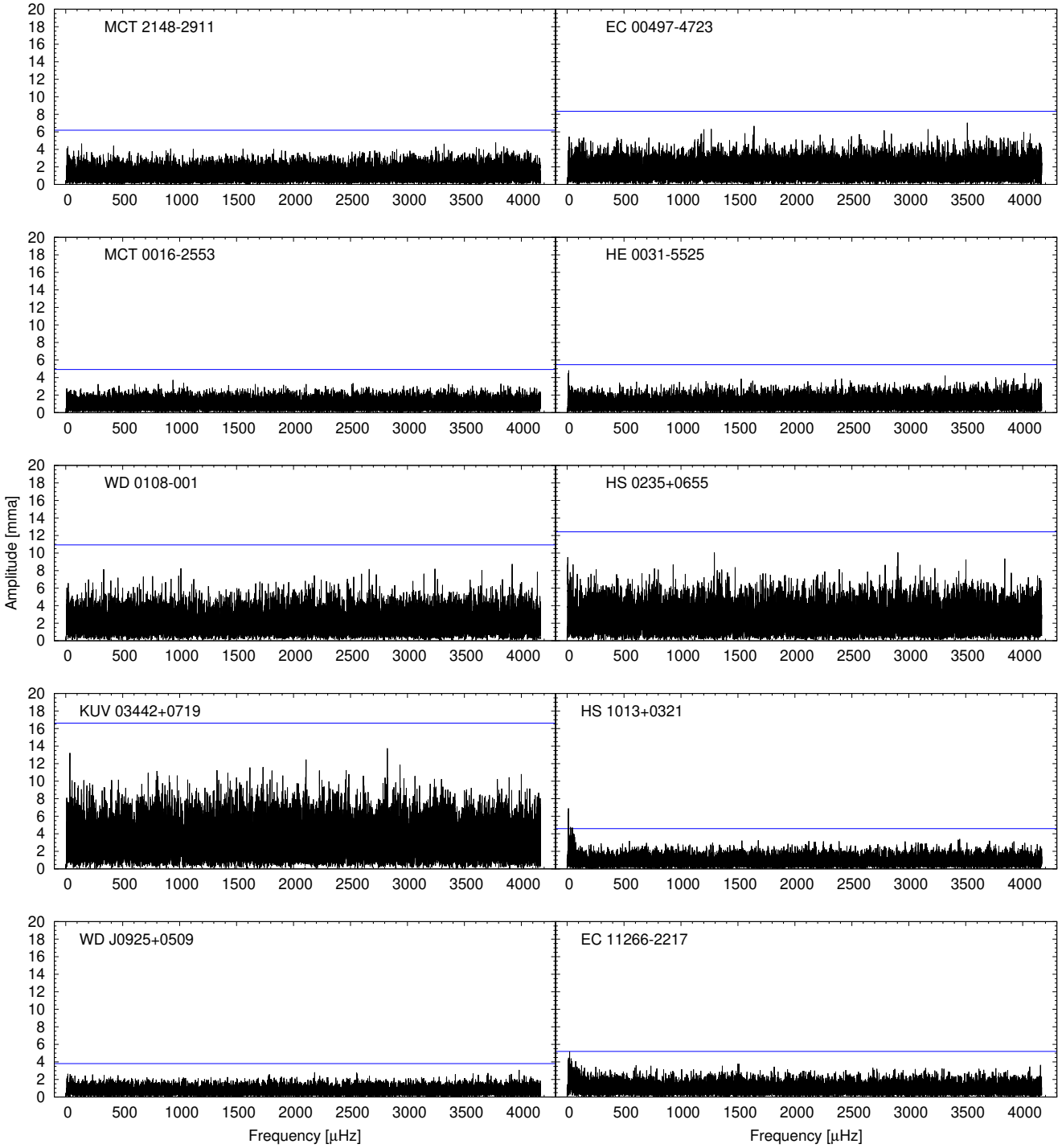

Fig. B.2. Fourier transforms of the ZZ Ceti stars not seen to vary by the TESS data. Blue lines denote the 0.1% FAP levels.